Hindawi Publishing Corporation
International Journal of Aerospace Engineering
Volume 2013, Article ID 859465, 24 pages
http://dx.doi.org/10.1155/2013/859465

Research Article

Film Cooling Optimization Using Numerical Computation of the Compressible Viscous Flow Equations and Simplex Algorithm

Ahmed M. Elsayed,[1] Farouk M. Owis,[2] and M. Madbouli Abdel Rahman[2]

[1] *Institute of Aviation Engineering & Technology, Giza, Egypt*
[2] *Aerospace Engineering Department, Faculty of Engineering, Cairo University, Giza, Egypt*

Correspondence should be addressed to Farouk M. Owis; fowis@eng.cu.edu.eg

Received 23 March 2013; Revised 24 June 2013; Accepted 1 July 2013

Academic Editor: Kenneth M. Sobel

Film cooling is vital to gas turbine blades to protect them from high temperatures and hence high thermal stresses. In the current work, optimization of film cooling parameters on a flat plate is investigated numerically. The effect of film cooling parameters such as inlet velocity direction, lateral and forward diffusion angles, blowing ratio, and streamwise angle on the cooling effectiveness is studied, and optimum cooling parameters are selected. The numerical simulation of the coolant flow through flat plate hole system is carried out using the "CFDRC package" coupled with the optimization algorithm "simplex" to maximize overall film cooling effectiveness. Unstructured finite volume technique is used to solve the steady, three-dimensional and compressible Navier-Stokes equations. The results are compared with the published numerical and experimental data of a cylindrically round-simple hole, and the results show good agreement. In addition, the results indicate that the average overall film cooling effectiveness is enhanced by decreasing the streamwise angle for high blowing ratio and by increasing the lateral and forward diffusion angles. Optimum geometry of the cooling hole on a flat plate is determined. In addition, numerical simulations of film cooling on actual turbine blade are performed using the flat plate optimal hole geometry.

1. Introduction

Over the past fifty years, aircraft and power generation gas turbine designers have focused on increasing the temperature at the combustor exit to improve the engine performance, to increase the thrust, and to reduce the fuel consumption. Unfortunately, these high temperatures have a negative effect on the integrity of the high-pressure turbine components specifically the turbine blades. Therefore, there is a need to have an efficient cooling system engineered in a way such that the maximum blade surface temperature during the engine operation does not exceed the maximum allowable temperature of the blade material.

To achieve this goal, several researchers such as [1, 2] focused on various innovative cooling techniques. Depending on the nature of the coolant flow, the cooling methods currently implemented in the turbine industry can be classified into two main categories which are the internal and external cooling as shown in Figure 1. In the first type cooler air is bled from the compressor stage and then passed through internal passages incorporated into blade designs for this purpose. This is the most common technique and is called enhanced passage cooling. For maximum heat absorption, the air is also allowed to impinge on the internal wall of the blade. This technique is called impingement cooling. In external cooling, air is bled from the compressor stage, ducted through the internal chambers of the turbine blades, and then discharged through small holes/slots on the blade outer walls. This air provides a thin, cooler and insulating film along the external surface of the turbine blade, due to which the method is called "film cooling." This film provides blade protection and thus increases the life of the blade.

To better understand film cooling, a simple case is considered where mainstream and air coolant are mixed up as shown in Figure 2. Heat flux represents the heat exchanged between the hot air and turbine blade. It is obvious that

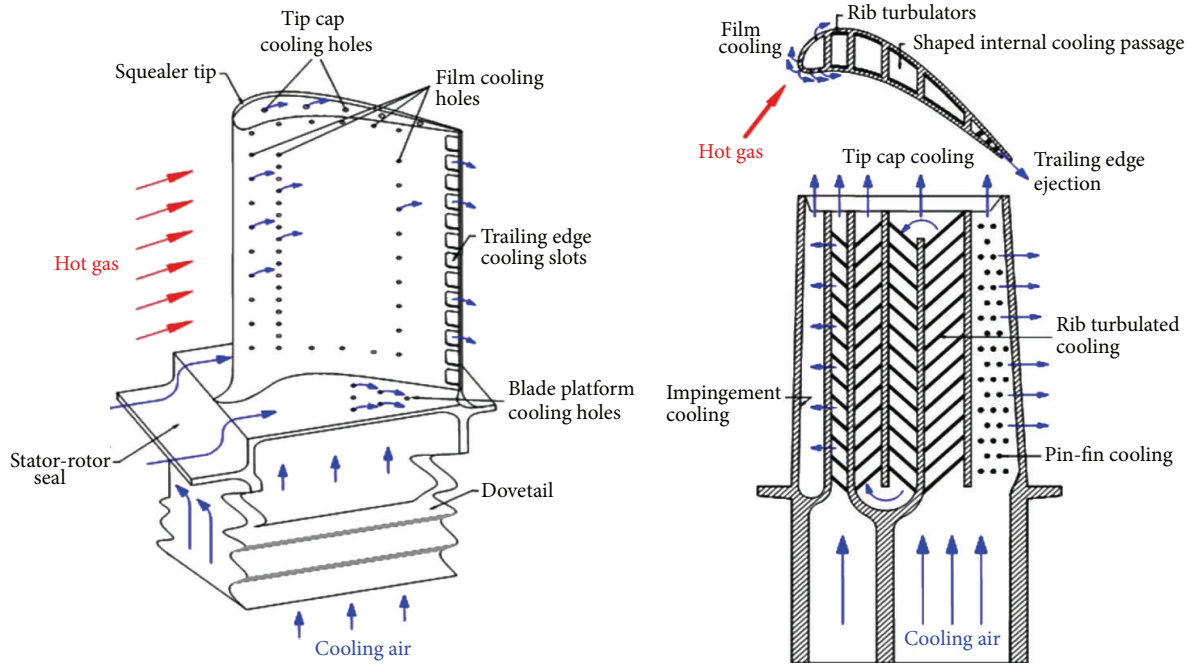

Figure 1: Gas turbine blade cooling schematic: (a) external cooling and (b) internal cooling.

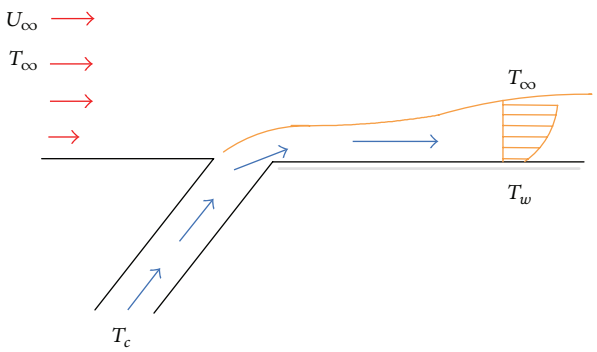

Figure 2: Protective film layer made by coolant injection.

keeping this value to a minimum is desirable. For this purpose, the introduced film cooling creates a protection zone between the hot air and surface of the blade.

Film cooling has been found to be very sensitive to many parameters such as the coolant-mainstream density, momentum and mass flux ratios, the mainstream turbulence intensity, mainstream passage/tip vortices, upstream wakes, surface curvature, and roughness. Thorough reviews of the parameters affecting film cooling are provided by Nasir et al. [3], Bogard and Thole [4], and Bunker [5].

The effect of coolant-mainstream blowing ratio is investigated by Rallabandi et al. [6]. The study by Rallabandi et al. [6] indicates that the nondimensional temperature and the film cooling effectiveness increase at low blowing ratios regardless of hole shape and injection angle. However, beyond a critical blowing ratio, film cooling effectiveness decreases. This result can be attributed to the phenomenon of film-cooling lift-off, where the high momentum jet fails to attach to the plate surface and the jet penetrates into the mainstream.

The coolant-mainstream density ratio (DR) in modern gas-turbine engines is typically around 2.0, due to the significantly lower temperature of the coolant. Scaled down laboratory tests, to simulate engines of different density ratio conditions, usually involve chilling the coolant to very low temperatures. In general, increasing density ratio at a given mainstream M results in a higher effectiveness, especially at higher blowing ratios, since the velocity of a high-density coolant is lower at a given M. Injecting the film coolant at an angle to the mainstream (a compound angle) results in higher film cooling effectiveness, due to a lower tendency to lift off. Embedding film cooling holes in slots as indicated by Bunker

[7] and Waye and Bogard [8] has been found to increase film cooling effectiveness in the proximity of the hole.

Multiple rows of film cooling holes are conventionally used in turbine blade designs. Ligrani et al. [9] studied typical distributions with both simple and compound angles. At lower blowing ratios, the effects of the numbers of rows are fairly insignificant. However, the double jet row shows higher effectiveness for high blowing ratios. More recently, Kusterer et al. [10] have studied two rows of film cooling holes with opposite orientation and internal supply geometries.

In the late 1960s, Goldstein et al. [11] studied the effect of lateral injection on film cooling effectiveness. Honami et al. [12] made simultaneous velocity and temperature measurements with one row of laterally injected jet issuing into a turbulent boundary layer. An asymmetric flow structure with a large-scale vortex motion is detected, which results in low film cooling effectiveness at increased blowing rate. Lee et al. [13] investigated the flow structure of one inclined injection hole with various orientation angles. A surface flow model is suggested.

Denton [14] suggests that despite an estimated increase in turbine entry temperature of 100 K per 1% coolant mass flow, a reduction of approximately 1% in turbine efficiency per 1% coolant flow can have a large effect on the overall cycle efficiency. This reduction is the viscous effect of irreversible mixing for the coolant and mainstream flows.

Ligrani et al. [15] present experimental results describing the flow structure and film cooling parameters downstream of a single row of holes with compound angle. Their results show that the compound angle injection configuration significantly improves the film cooling protection. In heat transfer measurements, Sen et al. [16] and Schmidt et al. [17] investigate the adiabatic wall effectiveness and heat transfer coefficient using a single row of inclined holes with different shapes, different compound angles, and a hole of length 4 d. Their results show that holes with a large compound angle had little effect on heat transfer rate for small momentum ratios, while heat transfer level is significantly increased for holes with compound angle at large momentum ratios. Ekkad et al. [18, 19] present film cooling effectiveness and heat transfer coefficient distributions over a flat surface with one row of inclined holes for three different compound angles and density ratios at an elevated freestream turbulence intensity to determine local effectiveness and heat transfer coefficient distribution simultaneously. The study indicates that compound angle injection provides higher effectiveness.

The interaction of the coolant jet with the crossflow produces a highly complex, three-dimensional flow field in the vicinity of the jet injection. The flow is characterized by both large-scale coherent structures and small-scale turbulence. The mixing process is controlled by the dynamics of these structures. The coherent structures of primary importance have been identified in the published literature to be jet shear-layer vortices, the horseshoe vortices, the counter-rotating vortex pair, and the wake vortices formed in the wake of the jet. The jet shear-layer vortices dominate the initial portion of the jet while the horseshoe vortices wrap around the base of the jet. The counter-rotating vortex pair results from the impulse of the jet on the crossflow. Accurate prediction of such structures is necessary to correctly predict the jet penetration and reattachment length that are important for heat transfer calculations and the optimization of film cooling effectiveness. Computations of flow and heat transfer for turbine rotor blade that has film cooling and high pressure gas are presented by Medic and Durbin [20] with an assessment of several turbulence models. Using the PSP technique Wright et al. [21] showed the result that free stream turbulence has upon cooling effectiveness, causing a spanwise spread in the film cooling effectiveness, though for high blowing rate jet lift-off prevents different turbulence levels from affecting the effectiveness much whatsoever. Muppidi and Mahesh's [22, 23] direct numerical simulation is used to study a round turbulent jet in a laminar crossflow, and they compared its mean velocity and turbulent intensities obtained from the simulations by published experiments data.

In the current study, film cooling on a flat plate is studied numerically to select the different parameters of the compound-hole shape that could enhance the cooling effectiveness. The flow on the flat plate with film cooling is numerically simulated using the steady, compressible Navier-Stokes equations with turbulence modeling. The flow solver is coupled with an optimization technique to obtain the cooling parameters. The simplex algorithm is used for the optimization procedures. The cooling-hole shape is defined in terms of four variables which are the streamwise angle (α), the lateral diffusion angle (γ), the forward diffusion angle (δ), and the coolant blowing ratio (M). The numerical simulations are performed for a single hole on a flat plate since the same effect can be obtained for more than one hole separated by an equal distance on a flat plate and applying symmetrical boundary conditions. However, it is difficult to simulate an array of holes on an actual 3D turbine blade as the shape varies along the blade height because of the blade twist and the effect of hub and tip section on the blade cooling. Therefore, optimization of film cooling parameters is done initially on a flat plate to obtain an initial shape of the holes for optimum film cooling on actual turbine blades.

The optimization process is carried out using "CFDRC package." The solver of this package ACE used the three-dimensional steady compressible viscous flow field coupled with the k-ε turbulence model. An unstructured grid is used for the simulations on the flat plate. The governing equations are discretized using the finite volume technique with second-order accuracy in space.

2. Numerical Model

2.1. Flat Plate Numerical Simulations. The film cooling on a flat plate is numerically simulated using the three-dimensional, steady, turbulent and compressible flow equations. The turbulence model k-ε is used in the simulation. The control volume of the flat plate model is illustrated in Figure 3. The cooling hole diameter (D) is selected to be 5 mm. The metering section length (L_1) and the diffusion section length (L_2) are assumed to be half the total length (L); that is,

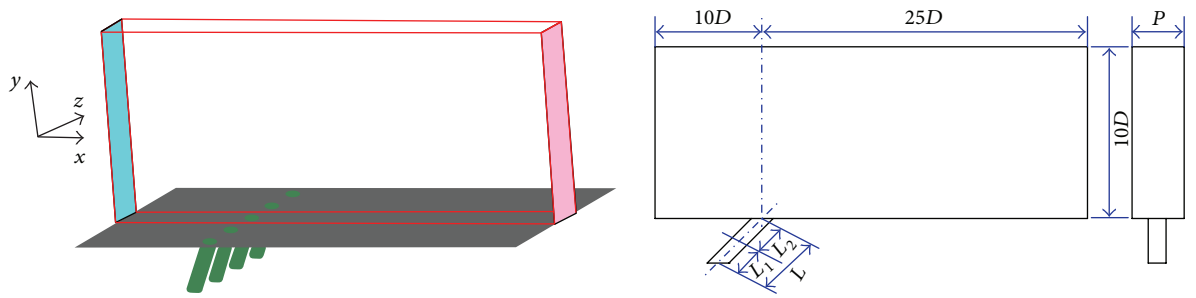

Figure 3: Flat plate numerical model.

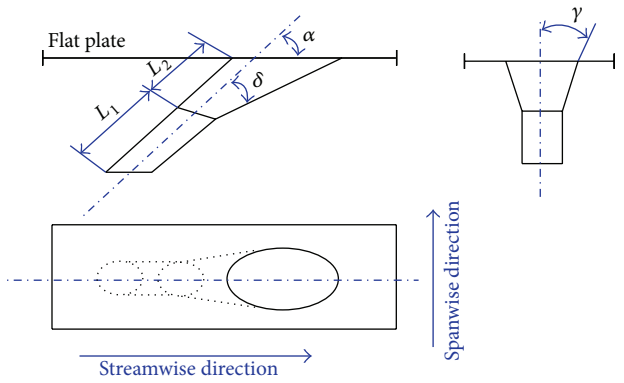

Figure 4: Generalized cooling hole configuration: LFDSA type.

$L_1 = L_2 = 0.5L = 1.5D$. The spanwise pitch (P) is taken to be three times the cooling hole diameter. The cooling fluid is injected to the mainstream at a streamwise angle (α) is varied from 20° to 90°, and a span wise angle (β).

2.2. Cooling-Hole Geometry. The selected geometry of the cooling hole is assumed to be the generalized laterally and forward-diffused (LFDSA) (also called fan-shaped laidback) type as shown in Figure 4. In the current study, the lateral diffusion angle (γ) and the forward diffusion angle (δ) varied from 0° to 15°. The hole configuration is nominated LFDSA-LL-FF, where LL and FF are the lateral and forward diffusion angles.

2.3. Boundary Conditions. Figure 5 presents the boundary condition of a flat plate model with system of holes. The mainstream gases are approximated as air with a temperature 333 K. The inlet mainstream flow is considered to have a uniform velocity of 10 m/s. The coolant inlet is taken to be air with a temperature 293 K. The inlet coolant flow is considered to have a uniform velocity. Density ratio is maintained at 1.14. For the specified blowing ratio, the inlet velocity of the coolant can be calculated. Symmetry boundary conditions are applied at the two vertical planes. The upstream and downstream surfaces of the flat plate are considered adiabatic. In addition, symmetrical boundary condition is applied at the upper boundary of the control volume since the gradients of flow field properties are considered to decay ten times the diameter of the hole.

2.4. Simplex Optimization Method. In the current work, the optimum hole shape of the flat plate film cooling is obtained using the simplex algorithm. Simplex is a simple optimization algorithm seeking the vector of parameters corresponding to the global extreme (maximum or minimum) of any n-dimensional function $F(x_1, x_2, \ldots, x_n)$, searching through the parameter space (search area). The cost function which is optimized in the current study is the average film cooling effectiveness.

The two-dimensional simplex starts with three observations of the system response obtained with three different parameter settings (guesses). These three observations correspond to the vertices of a triangle constituting the first simplex. In three-dimensional space, four initial observations defining a tetrahedral body are required. For spaces higher than three dimensions, the procedure is valid, even though it becomes difficult to visualize.

The simplex algorithm procedures are as follows.

(1) Provide a value for Delta (first step size) for the optimizer to construct the first simplex which is used to start the optimization process. Delta and initial value for each of the two variables are used to create the first three points (B, NB, and W), the left of Figure 6.

(2) The position of the centroid is then calculated. CEN is located between the best point B and next to best point NB.

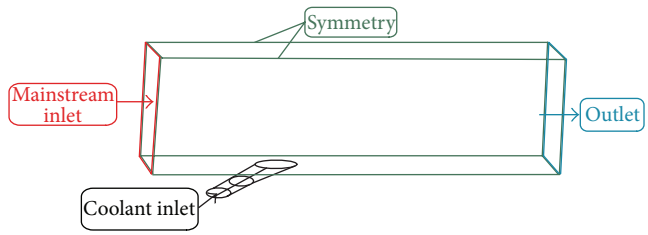

Figure 5: Model boundary conditions.

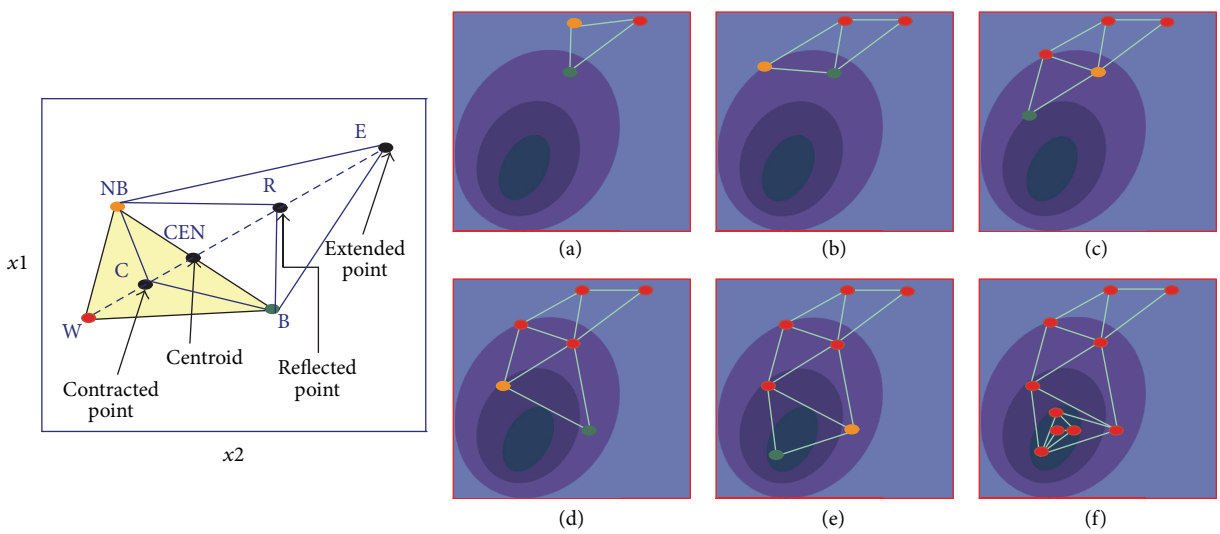

Figure 6: Reflection, expansion, or contraction operations on search area of 2D simplex.

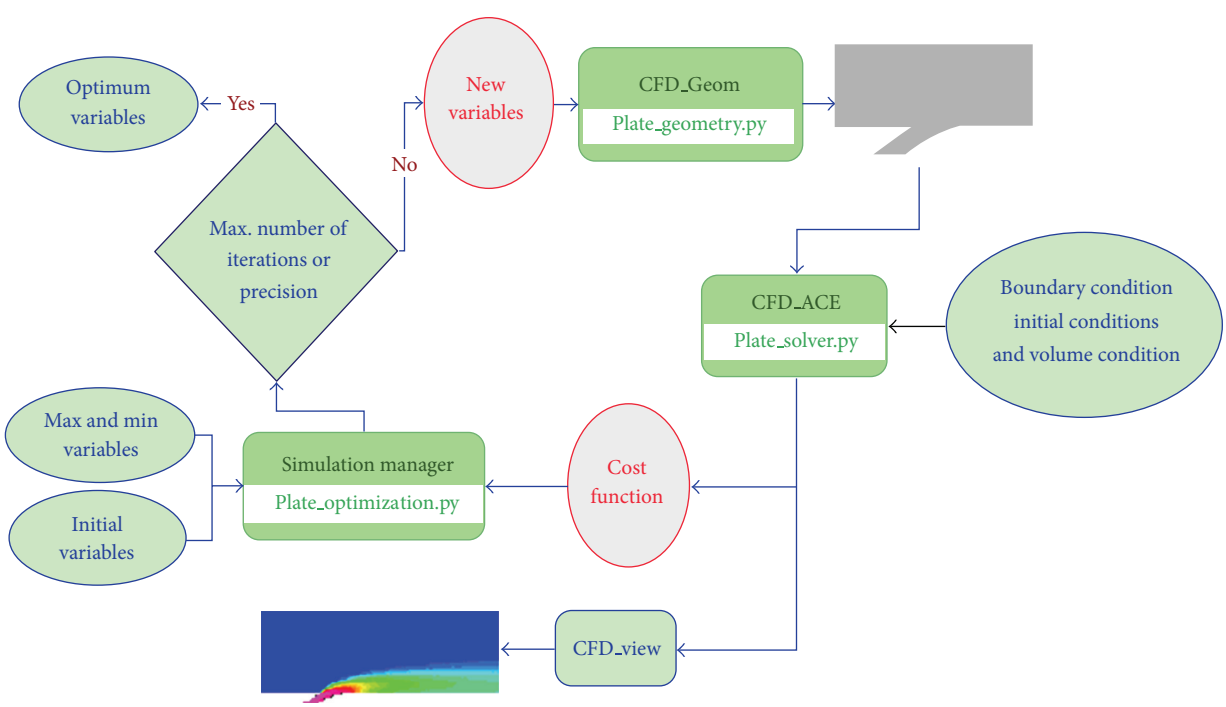

Figure 7: Optimization loop of CFD-ACE package.

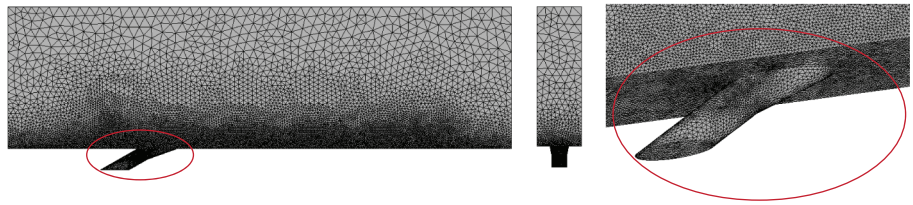

Figure 8: Unstructured grid used for the LFDSA-5-5 hole with a minimum cell size of 0.4 mm and a maximum cell size of 2.4 mm.

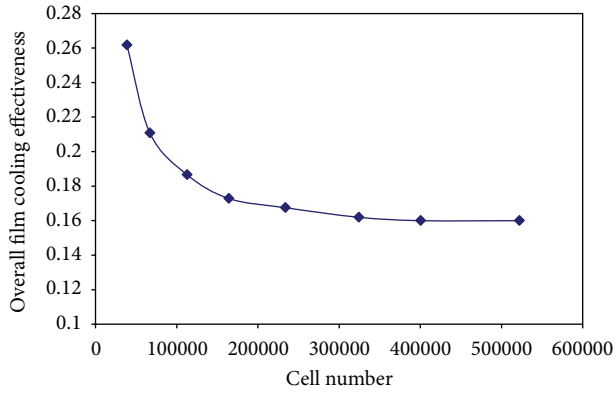

Figure 9: Variation of the average film cooling effectiveness with the grid size for $M = 1$.

(3) A reflection through CEN of the worst-response point W is performed, and the response RR of the reflected point R is evaluated.

(4) If R is within the search area and its response RR is better than RW but not better than RB, then a new simplex is formed by replacing W with R. The process is repeated from Step (1) with the new simplex.

(5) If the response of R, RR, is even better, that is, better than RB, then this is an indication that the simplex is moving in the correct direction. Hence an extension to point E is tried (E is twice as far from CEN as R in the same direction).

(6) If E is within the search area and its response RE is better than RR, then W is replaced with E; otherwise W is replaced with R. The process is repeated from Step (1) with the new simplex.

(7) If the initial reflection fails, that is, RR is worst than RW, or R is not within the search area, then a contraction is performed. The contracted point C (located midway between W and CEN) replaces W. The process is repeated from Step (1) with the new simplex and so on.

A two-dimensional simplex algorithm example shows the procedures of optimization which are started by constructing the first triangle at (a) and followed by a reflection, expansion, or contraction triangle inside the search area until reaching the maximum value of cost function (dark blue color) at (f) as shown in Figure 6.

The optimization procedures are carried out by developing three programs written in the PYTHON programming language (geometry file, solver file, and optimization or control file). Figure 7 presents the optimization procedures which are started by defining the following variables in the control file:

(i) the initial variables;

(ii) the variables limits (maximum and minimum);

(iii) the maximum number of iterations for the optimization cycle (100 iterations for the case study);

(iv) precision (10^{-3} for the case study);

(v) the step size of each variable (20% is the difference between the maximum and minimum values of each variable).

3. Results

3.1. Unstructured Grid Sensitivity Analysis. A grid size function is used to adjust the grid size near the boundaries. The size function applied has a minimum cell size of 0.4 mm at a high curvature area and a maximum cell size of 2.4 mm at low curvature area (straight area). The growth rate factor is used to adjust the grid number between the two areas. The unstructured grid for the simulation of the film cooling using the LFDSA-5-5 hole is presented in Figure 8.

A grid sensitivity analysis for a case study having LFDSA-5-5 hole shape with streamwise angle equal to 30 deg is performed for a specified blowing ratio M which is defined as follows:

$$M = \left(\frac{\rho_c v_c}{\rho_h v_h} \right). \quad (1)$$

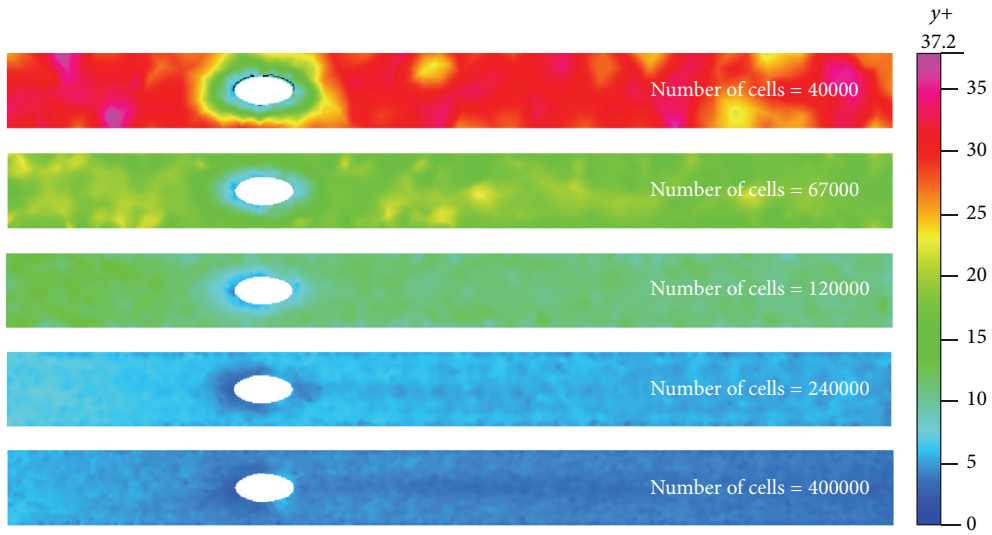

Figure 10: Contours of $y+$ on the wall for different numbers of grid cells.

The results of the grid sensitivity analysis are shown in Figure 9 in terms of the non dimensional average wall temperature. The average overall film cooling effectiveness is defined as follows:

$$\eta_o = \left(\frac{T_h - T_{\text{av}}}{T_h - T_c} \right). \quad (2)$$

The results presented in Figure 9 indicate that the average film cooling effectiveness slightly changes for a grid size greater than 400000 cells. In addition, Figure 10 presents the nondimensional quantity ($y+$) which expresses the density of grid on the flat plate wall surface with a hole of different numbers of control volume cells. It is clear from the figure that the density of grid zone has smaller value of $y+$ compared to the other area in the different cases for a grid size of 400000 cells. The maximum value of $y+$ does not exceed the value of 5 for this grid.

Figure 11 presents the effect of varying the number of cells in the streamwise direction. The profiles of the film cooling effectiveness are shown at different cutting lines in the plane of symmetry ($Z = 0$) for a case study having LFDSA-5-5 hole shape with streamwise angle of 30 deg and blowing ratio of 1. The figure indicates that the wall centerline film cooling effectiveness or the film cooling layer thickness increases in streamwise direction with different numbers of cells up to a grid size of 400000. The results do not change much for grid size greater than 400000. Thus, this grid size is considered to be enough for accurate simulations.

In addition, Figure 12 presents the film cooling effectiveness variation in the spanwise direction (Z). The film cooling effectiveness has a maximum value at the flat plate centerline along streamwise direction, and this value decreases in spanwise direction. The results indicate that the suitable number of cells for accurate simulations is 400000 cells.

3.2. Verification of Numerical Model. The film cooling on a flat plate with an injection hole of shape LFDSA-00-00 (CYSA) is simulated numerically, and the results are compared with Daud et al. [24], Ai et al. [25], Nasir et al. [26], and Kline et al. [27]. The simulations of this CYSA hole shape are calculated on unstructured grid and RNG turbulent model. The same boundary conditions of Daud are used in the current simulations. The mainstream inlet flow is assumed to have a temperature of 302 K and a uniform velocity of 18 m/s. The temperature of the coolant inlet flow is assumed to be 153.3 K. The simulations performed by Daud using Fluent for a structured grid and RNG turbulent model. The results are compared with those computed by Daud as shown in Figure 13. The results show good agreement.

The current results of the local film cooling effectiveness using the CFDRC package with unstructured grid for two different turbulent models (k-ε and RNG) are compared with the previous theoretical results by Daud et al. [24] and Liu et al. [28] and experimental results by Sinha et al. [29] at two different positions as shown in Figure 14. A structured grid and RNG turbulent model are used by Daud et al. [24] and Liu et al. [28]. The current results show good agreement with the previous numerical simulations and the experimental data. In addition, the results along the plate (x-direction) indicate that the k-ε model has good agreement with the experimental data and the previous simulations. The RNG model is better than k-ε model in the mixing region between the mainstream and cooling flow.

3.3. Parametric Study of Film Cooling on a Flat Plate

3.3.1. Effect of Coolant Inlet Velocity Direction. The effect of the cooling velocity direction on the film cooling effectiveness is investigated for a streamwise angle of 30 deg. Two different velocity directions are used for the coolant injection as shown

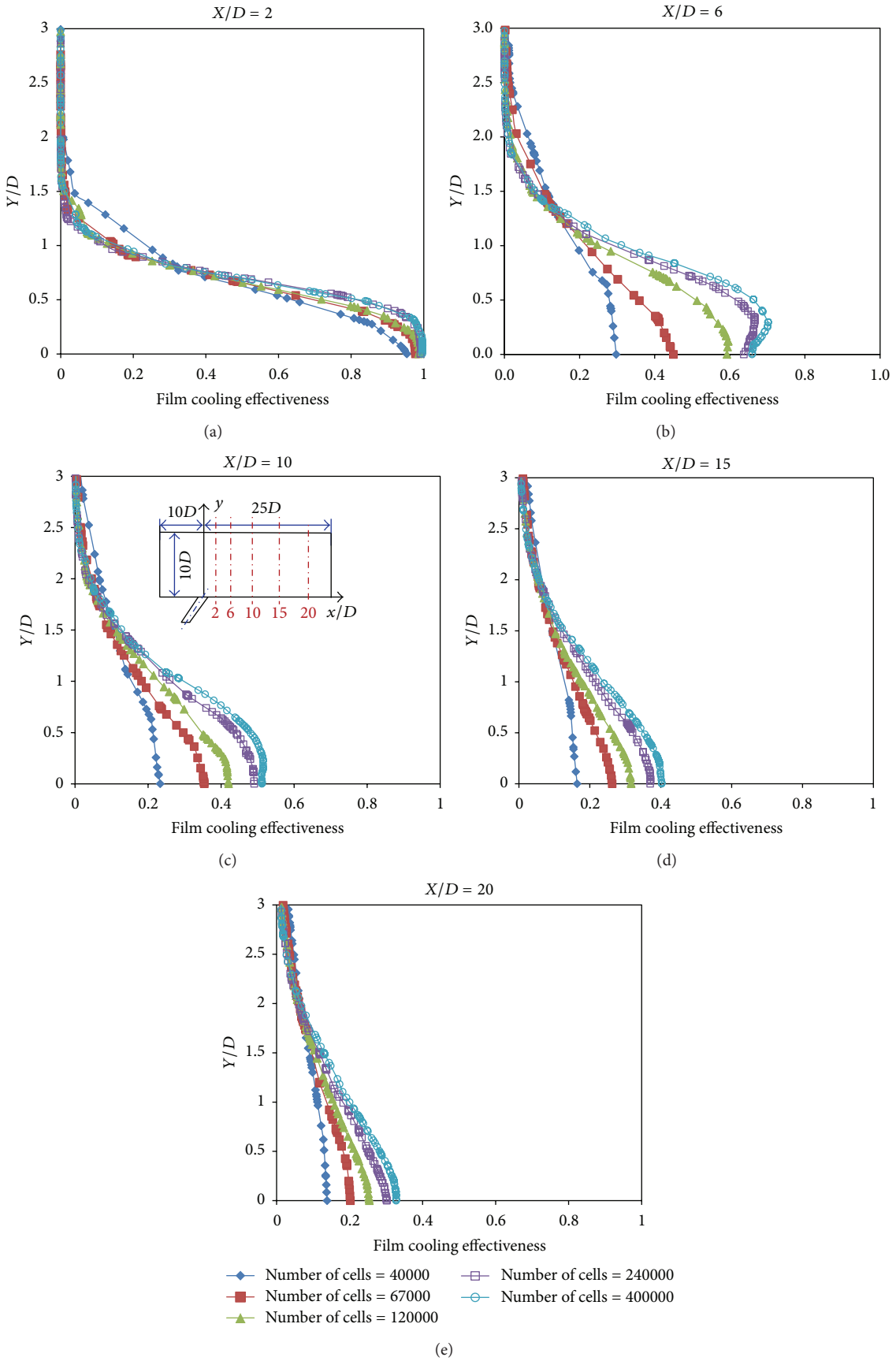

Figure 11: Variation of the wall local film cooling effectiveness with the number of cells.

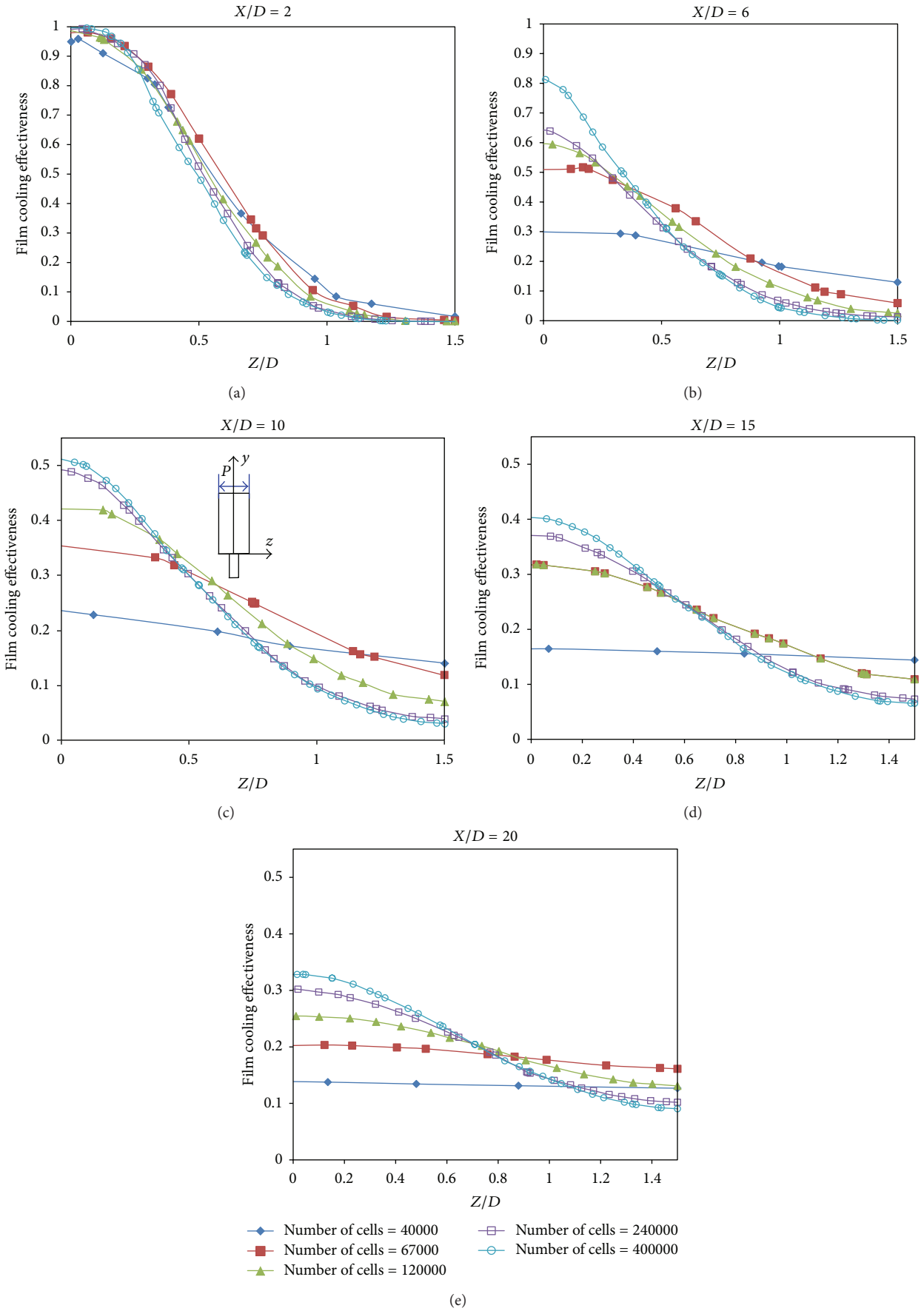

Figure 12: Variation of the local film cooling effectiveness with the spanwise direction for LFDSA-5-5 hole, streamwise angle 30 deg, and $M = 1$.

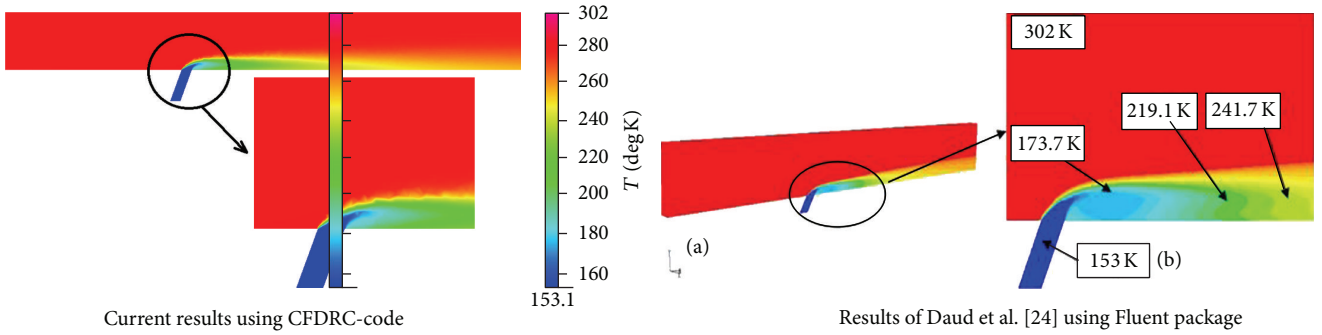

Figure 13: Comparison of static temperature contours of a single cylindrical hole.

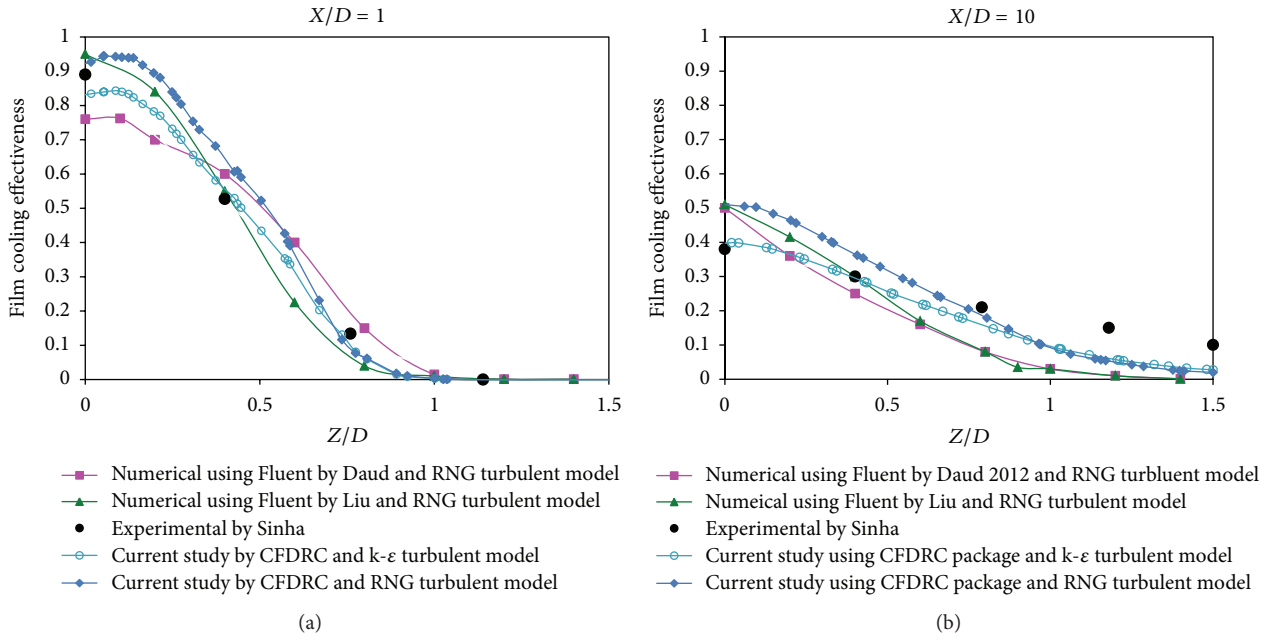

Figure 14: Variation of local film cooling effectiveness with the spanwise direction at two different positions of (X/D).

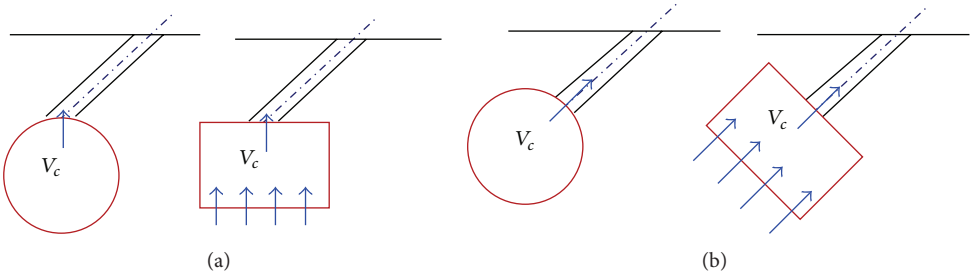

Figure 15: Schematic of two model inlet cooling flow directions.

in Figures 15(a) and 15(b). In Figure 15(a), the coolant flow is assumed to be normal to the plenum of value V_c and a streamwise angle of 60 degrees; while, in Figure 15(b), the flow is assumed to be normal to the plenum with the same value of cooling velocity V_c.

It is clear from the results shown in Figure 16 that the film cooling effectiveness has no lift-off for the two cases for low blowing ratio of 0.45 and the plate wall is well covered along the centerline. For the case of the velocity direction being normal to the hole, the coolant penetrates deeper into the mainstream flow in the longitudinal coverage than the case of the cooling velocity being in the streamwise direction. At blowing ratio of 1, a small lift off occurred for the case of velocity normal to hole inlet, and the plate wall is well covered

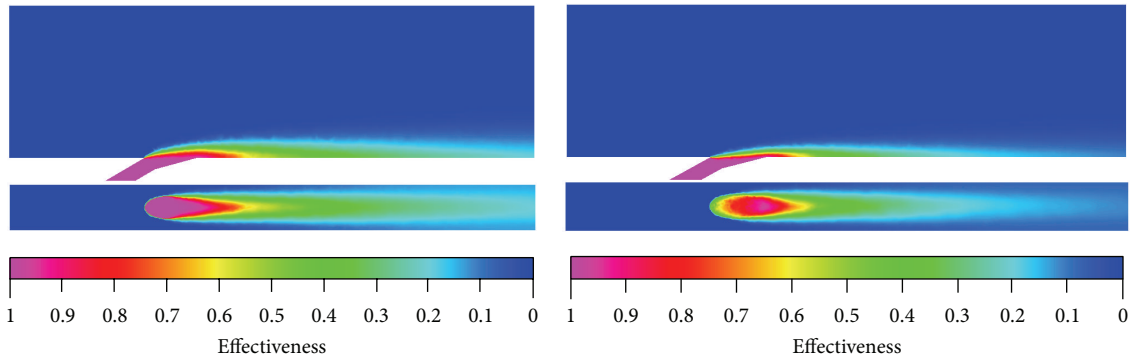

(a) Coolant velocity normal to boundary (b) Coolant velocity in the direction of streamwise angle

Figure 16: Top and symmetric planes of LFDSA 15-15 and $M = 0.45$.

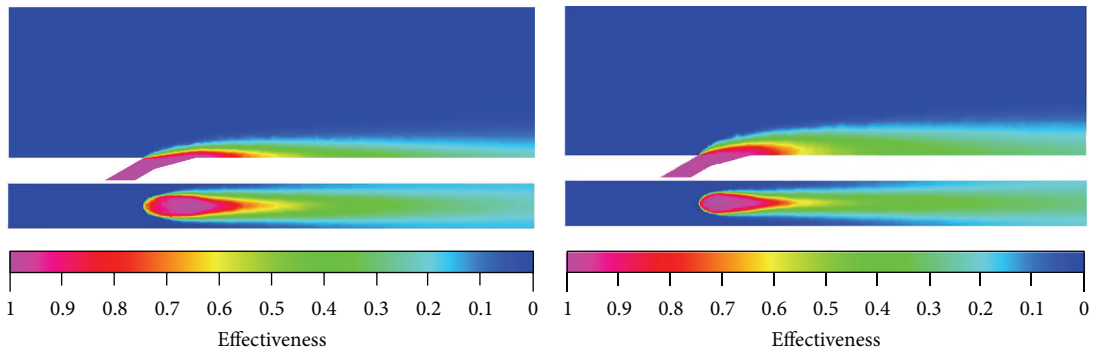

(a) Coolant velocity normal to boundary (b) Coolant velocity in the streamwise direction

Figure 17: Top and symmetric planes of LFDSA 15-15 and $M = 1$.

along the centerline as shown in Figure 17(a). Lift off does not exist for the case in which the coolant gas is injected parallel to streamwise angle. In this case, the plate wall is very well covered along the centerline as shown in Figure 17(b).

At blowing ratio 2 and cooling velocity normal to the hole inlet, higher values of lift off exist and the plate wall is not well covered along the centerline as shown in Figure 18(a). While for a velocity parallel to streamwise angle the lift off does not occur and the plate is well covered with cooling air as shown in Figure 18(b).

The velocity vectors and their magnitudes inside the injection hole are shown in Figure 19 to describe a stratification of the kinetic energy inside the hole. When the velocity direction is normal to the boundary, the results demonstrate that most of the fluid is impinging at a high velocity on the left half of the tube. In the right half, the entrained fluid is creating a small recirculation.

At low blowing ratio 0.45, the fluid which leaves the hole is spilled over the plate surface. The jet body is not detected, and the plate wall is very well covered along the centerline. At blowing ratio 1, the jet body becomes recognizable inside the left half of cooling hole that increases a vertical velocity component at the hole exit leading edge. In the right half, the entrained fluid is creating more recirculation as shown in Figure 19(b) that is increasing impingement of the air cooling on the plate surface. Thus, the plate surface is protected from the hot gases. At blowing ratio 2, the jet body becomes very recognizable inside the left half of cooling hole that increases the vertical velocity at the leading edge of the hole exit. In the right half, the entrained fluid is creating a separation from the plate surface that decreases the velocity at the trailing edge of the hole exit, and the influence of the imperfection is strong. The lift off phenomenon occurs as shown in Figure 19(c).

When the velocity direction is parallel to the streamwise angle, the results indicate that most of the fluid is impinging at a high velocity on the right half of the hole. In the left half, the entrained fluid is creating a small recirculation. At the low blowing ratio 0.45, the jet body is not detected and the plate wall is very well covered along the centerline. The penetration of the cooling flow in the longitudinal coverage is less than that in the first case (velocity direction is normal to the boundary) as shown in Figure 20(a). At blowing ratios of 1 and 2, the jet body is not detected. The velocity increases in the trailing edge of the hole exit, and a small recirculation exits in the leading edge as shown in Figure 20. The plate wall is very well covered along the centerline, and the lift off decreases.

The velocity profile at different sections in the streamwise direction is presented in Figure 21. The figure indicates that the mixing of cooling with the mainstream flow is improved

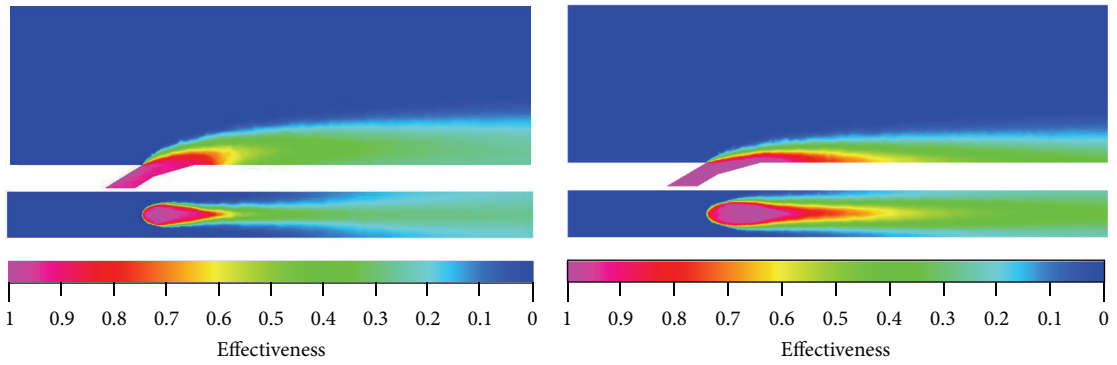

(a) Coolant velocity normal to boundary

(b) Coolant velocity in the streamwise direction

Figure 18: Top and symmetric planes of LFDSA 15-15, $M = 2$ for different coolant velocity direction.

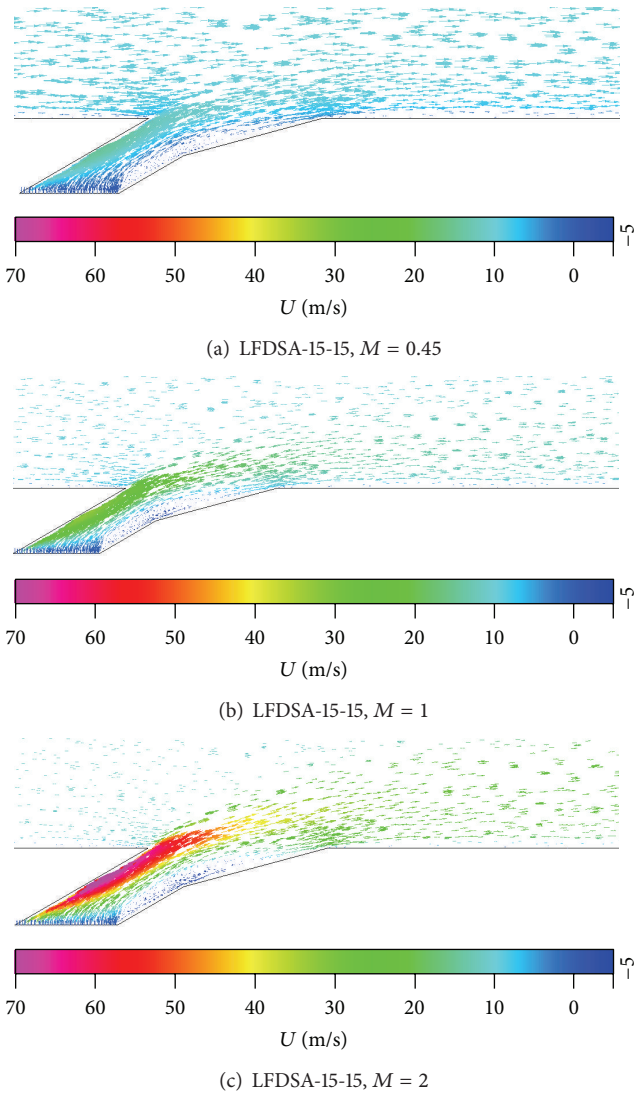

(a) LFDSA-15-15, $M = 0.45$

(b) LFDSA-15-15, $M = 1$

(c) LFDSA-15-15, $M = 2$

Figure 19: Velocity vectors on a symmetric plane and the coolant velocity normal to boundary.

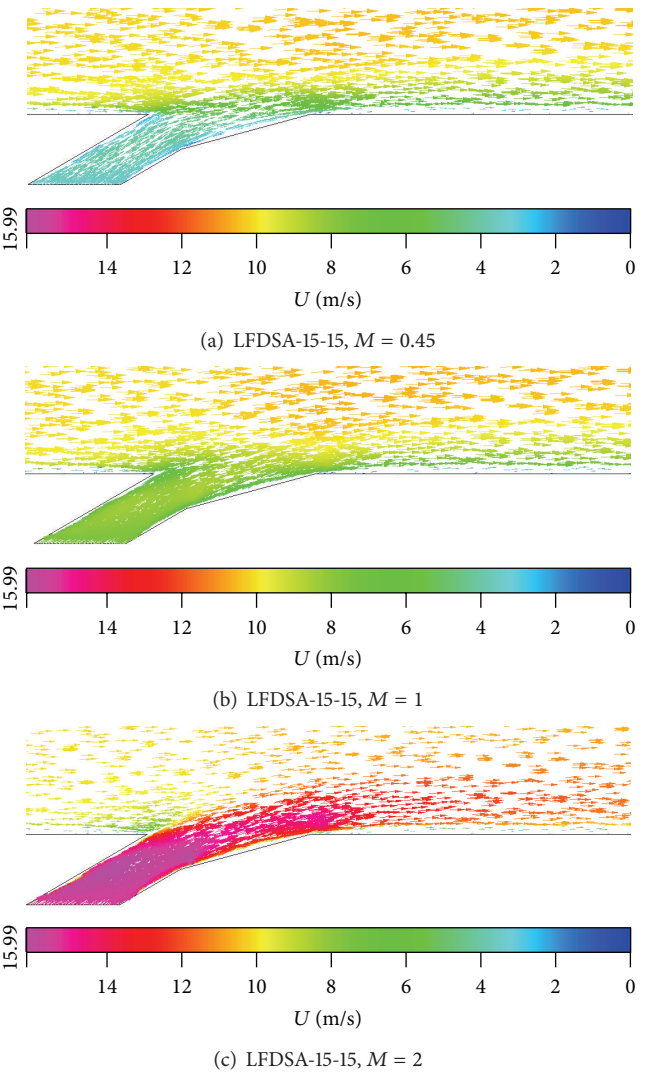

(a) LFDSA-15-15, $M = 0.45$

(b) LFDSA-15-15, $M = 1$

(c) LFDSA-15-15, $M = 2$

Figure 20: Velocity vector on a symmetric plane for a velocity in direction of streamwise angle.

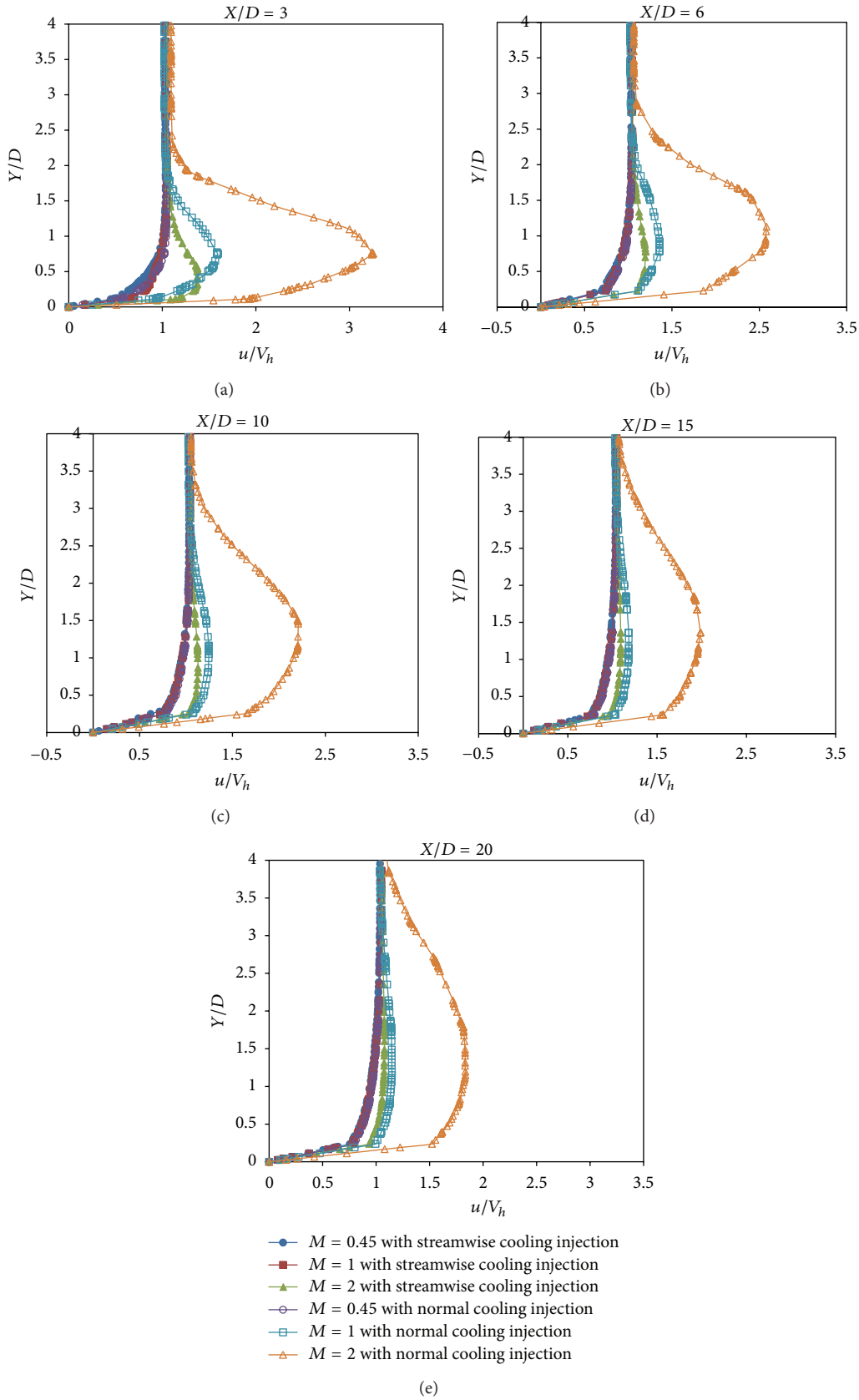

Figure 21: Velocity profile at the wall centerline for LFDSA-15-15 and different blowing ratios.

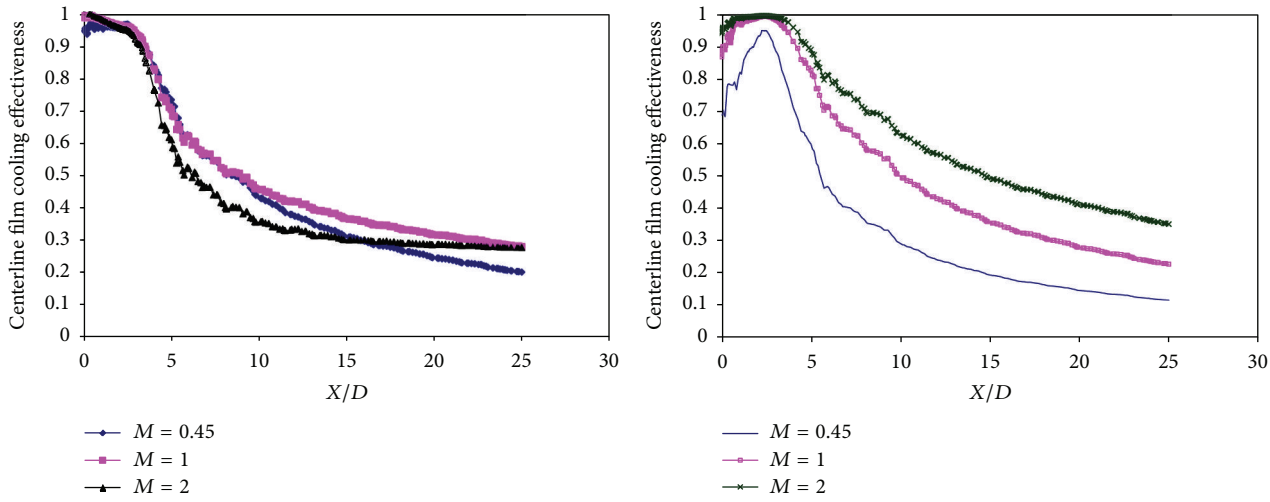

(a) Coolant velocity normal to boundary

(b) Coolant velocity in direction of streamwise angle

FIGURE 22: Centerline effectiveness versus X/D of LFDSA-15-15 hole shape for different blowing ratios.

along the streamwise direction. In addition, the velocity profile in case of inlet cooling flow being injected normal is fatter than the case of inlet streamwise cooling injection for different values of blowing ratio along the streamwise direction, especially at $M = 2$ and the velocity profile becomes very fat behind the wall which means not sufficient mixing with high strength of counter-rotating vortex pair and high lift off on the wall.

The effect of the blowing ratio on the centerline longitudinal effectiveness is presented in Figure 22 for the two aforementioned cases of the velocity direction. For a velocity direction parallel to streamwise angle, film cooling effectiveness is increasing as the blowing ratio increases while the blowing ratio has a little effect on the cooling effectiveness for a velocity direction normal to the hole inlet on the opposite for the case of a velocity direction parallel to the streamwise angle.

The variation of lateral angle with cooling flow injected in the streamwise direction has a great effect on the film cooling effectiveness in streamwise and spanwise directions, and this variation depends on the value of cooling blowing ratio. By increasing the lateral angle the effectiveness has a wider region on the wall. This diffused shape decreases the lift off at the mixing region with the mainstream flow, and it helps in covering a long area of streamwise direction with cooling flow in addition to a good cooling in spanwise direction. But the high increase in the lateral angle decreases the forward cooling velocity, so the mixing between the cooling flow and mainstream flow becomes very bad in streamwise direction but with a good cooling in spanwise direction. Figure 23 presents the streamwise and spanwise ($X/D = 2$) film cooling effectiveness of different lateral angles with forward angle equal to 15 degrees and streamwise angle equal to 30 degrees at different values of blowing ratio. At law value of blowing ratio, $M = 0.45$, with LFDSA-0-15 (FDSA) a good cooling at the centerline hole exit area but with a rapid decrease in cooling in spanwise direction and good cooling in streamwise direction compared to the other cases, the LFDSA-10-15 shape has a good cooling at the centerline hole exit area and spanwise and streamwise directions. The worst case cooling in the centerline hole exit and streamwise direction at this blowing ratio for a high lateral angle LFDSA-15-15 shape which has a lower forward cooling flow but with deeper cooling in spanwise direction. For high values of blowing ratio, an improvement in spanwise film cooling effectiveness by increasing the lateral angle with an improvement also in streamwise film cooling effectiveness up to $\gamma = 10$ degrees. If the lateral angle increases greater than this value, the streamwise film cooling effectiveness decreases about the streamwise effectiveness which is obtained with $\gamma = 0$.

3.3.2. Effect of Streamwise Angle. The streamwise angle has a significant effect in momentum exchange between the mainstream flow and the cooling flow on the film cooling effectiveness for high blowing ratios. At low blowing ratio 0.2 the effect of streamwise angle is small due to low value of coolant mass flow rate as shown in Figure 24. As the blowing ratio increases for row of jets of a given streamwise angle, the effectiveness near the holes increases up to a certain value at which the jets start to lift off, and the effectiveness decreases. Optimum blowing ratios can be clearly seen in Figures 25, 26, and 27 where jet lift-off does not exist. Maximum film cooling effectiveness for different values of blowing ratio occurs at a streamwise angle of 30 degrees which has a high rate of momentum exchange between the mainflow and the cooling flow and better cooling.

The effect of blowing ratio on centerline effectiveness up to $25D$ downstream of the cooling hole is shown in Figure 28, for different streamwise angles of LFDSA-00-00 configuration. At this case of studding, it is found that at law blowing ratio ($M = 0.2$) the centerline effectiveness approximately the same along chord length (x) for different

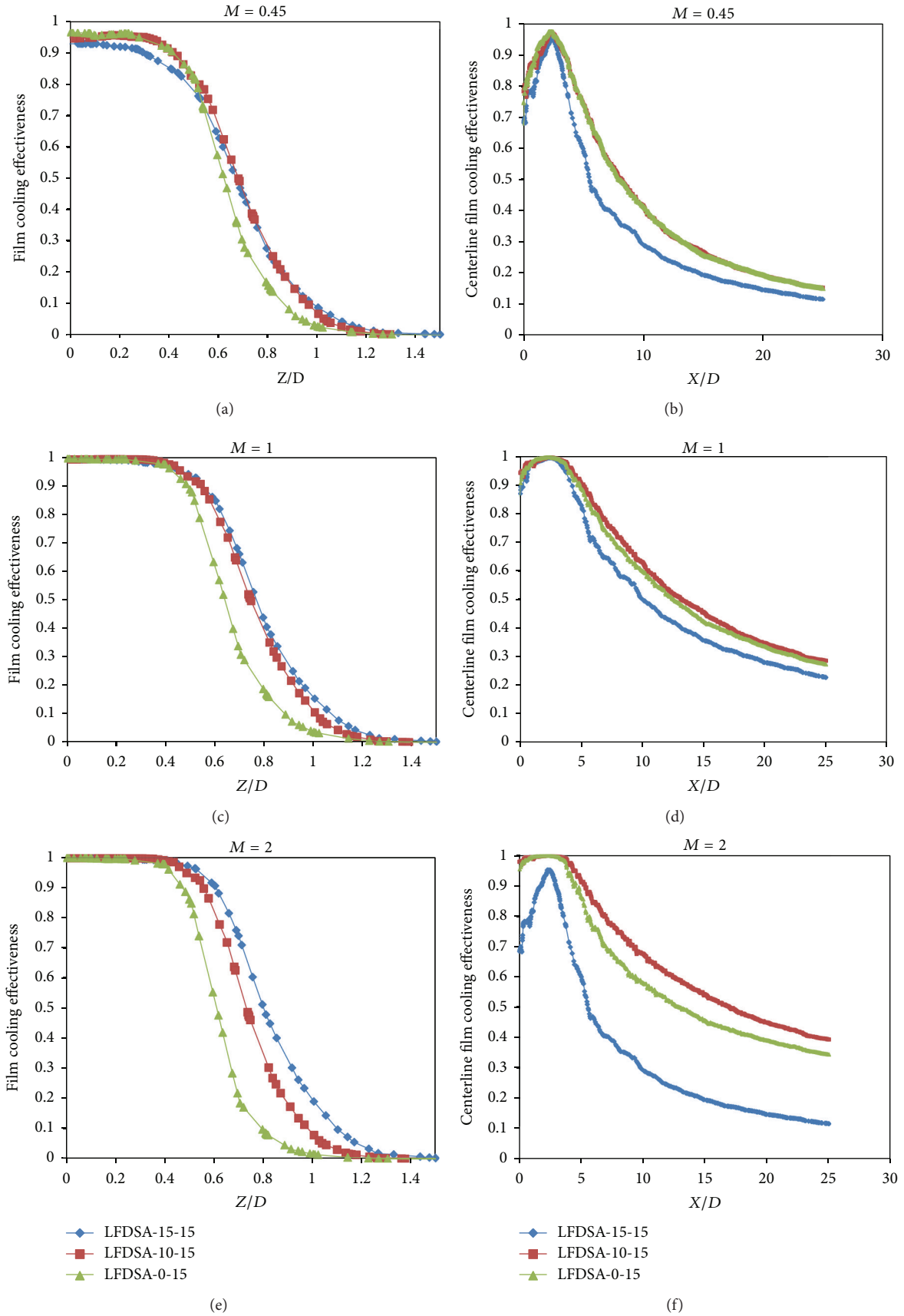

Figure 23: Effect of hole lateral angle on streamwise and spanwise ($X/D = 2$) film cooling effectiveness for cooling hole forward angle of 15 deg and streamwise angle of 30 deg.

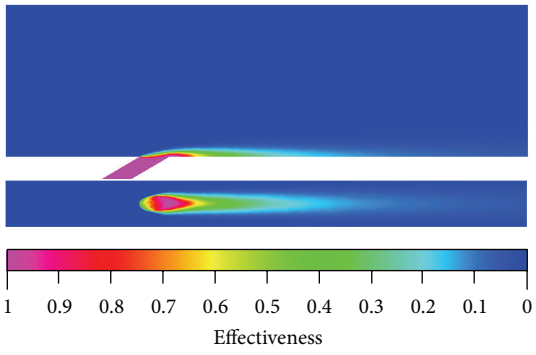

(a) LFDSA-00-00, $\alpha = 30^{\circ}$

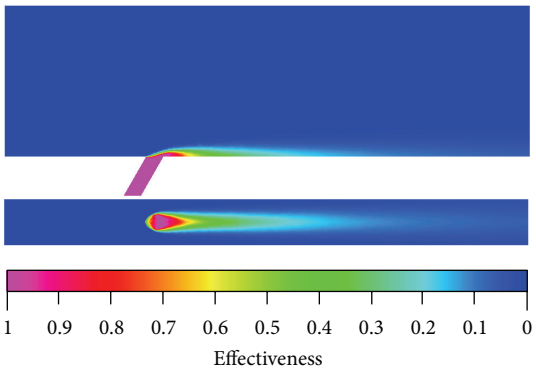

(b) LFDSA-00-00, $\alpha = 60^{\circ}$

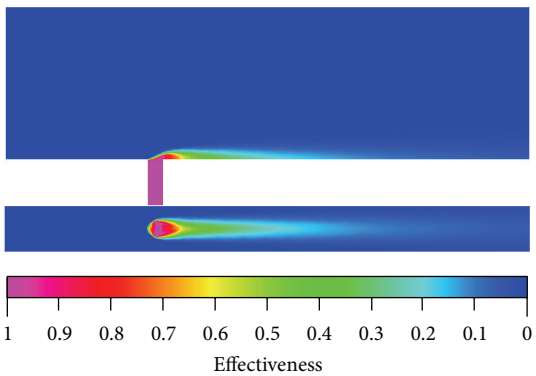

(c) LFDSA-00-00, $\alpha = 90^{\circ}$

FIGURE 24: Top and symmetric planes effectiveness of LFDSA-00-00 for different streamwise angles and $M = 0.2$.

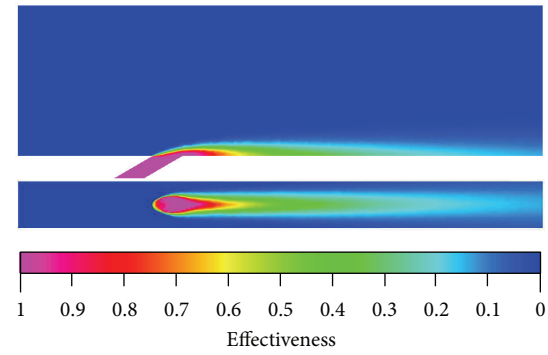

(a) LFDSA-00-00, $\alpha = 30^{\circ}$

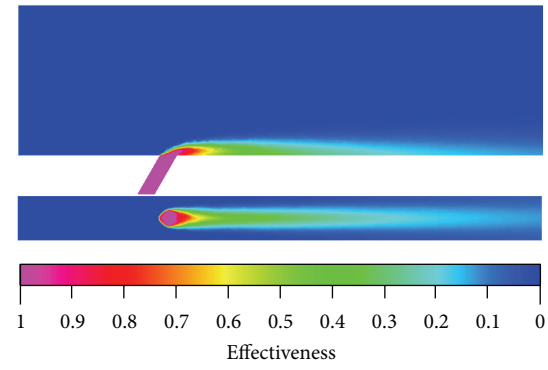

(b) LFDSA-00-00, $\alpha = 60^{\circ}$

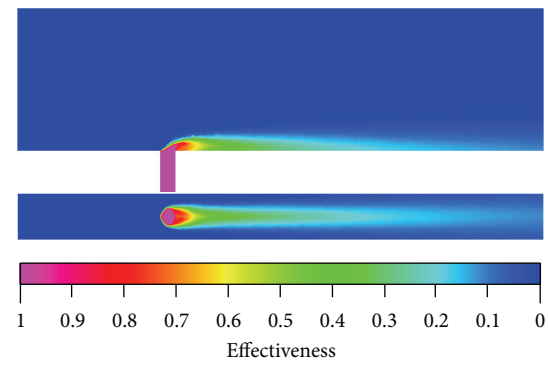

(c) LFDSA-00-00, $\alpha = 90^{\circ}$

FIGURE 25: Top and symmetric planes effectiveness of LFDSA-00-00 for different streamwise angles and $M = 0.45$.

streamwise angles due to low mass flow rate incoming from the cooling hole. As the blowing ratio is increased to $M = 0.45$, the centerline effectiveness increases slightly especially for small streamwise angles. This increase differs from a low value streamwise angle ($\alpha = 30$ deg) and a high value of streamwise angles ($\alpha = 60$ and 90 deg). At $M = 1$, the lift off phenomena appears for the high values of streamwise angles and the centerline effectiveness decreases. By increasing the value of blowing ratio ($M = 2$), the centerline effectiveness has a low value at the beginning of chord length; this value increases with the increase in chord length.

The structure of the film cooling flow is examined to study the effect of counter-rotating vortex pair (CRVP) on the film cooling. Traditionally, the coolant's momentum flux ratio is thought to be the most critical parameter for film cooling effectiveness. However, the index of film cooling performance is also influenced notably by counter-rotating vortex pair. The sources of CRVP are the in-tube vortex, the in-tube boundary layer vorticity, and the jet/mainstream interaction effect alone or combined. By simulating a general inclined cylindrical cooling hole on a flat plate, the CRVP was visualized as well as the interaction of mainstream and coolant stream

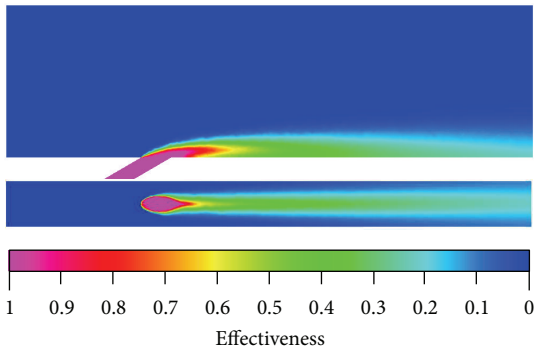

(a) LFDSA-00-00, $\alpha = 30^{\circ}$

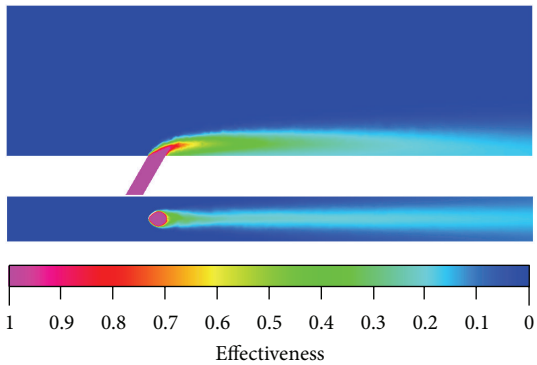

(b) LFDSA-00-00, $\alpha = 60^{\circ}$

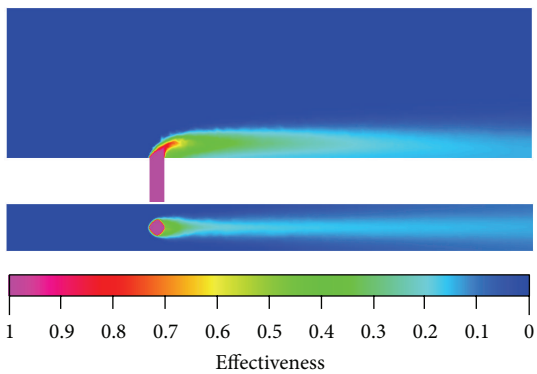

(c) LFDSA-00-00, $\alpha = 90^{\circ}$

FIGURE 26: Top and symmetric planes effectiveness of LFDSA-00-00 for different streamwise angles and $M = 1$.

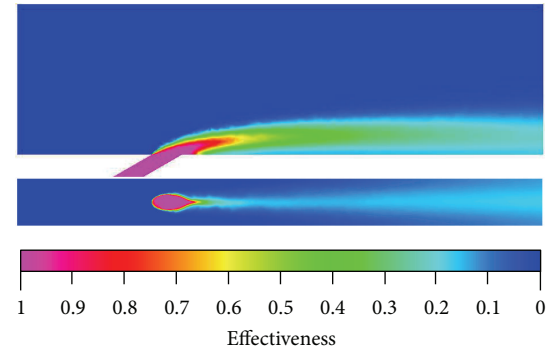

(a) LFDSA-00-00, $\alpha = 30^{\circ}$

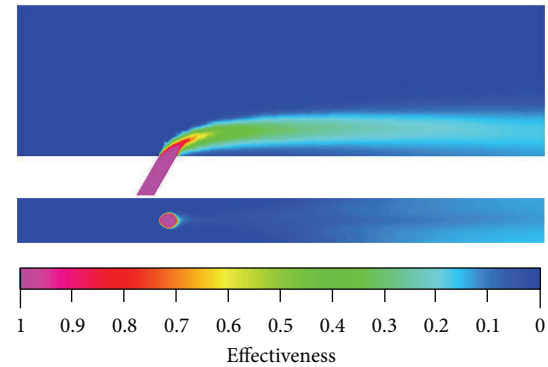

(b) LFDSA-00-00, $\alpha = 60^{\circ}$

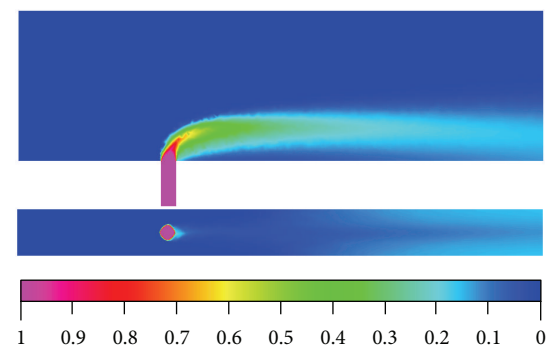

(c) LFDSA-00-00, $\alpha = 90^{\circ}$

FIGURE 27: Top and symmetric planes effectiveness of LFDSA-00-00 for different streamwise angles and $M = 2$.

tubes as indicated in Figure 29. This figure presents the stream tubes of different streamwise angles of LFDSA-0-0 with different blowing ratios. The jet/mainstream interaction is the only essential source of counter-rotating vortex pair. At blowing ratio 1 and streamwise angle of 30 degrees, a good mixing between the mainstream and coolant flow due to the counter-rotating vortex pair without lift off is noticed which results from the impulse of the jet on the crossflow. The wake vortices formed are weak. The strength of the counter-rotating vortex pair increases by increasing the streamwise angle. At streamwise angle of 90 degrees, the counter-rotating vortex pair is strong due to high coolant momentum flux in vertical direction which causes the cooling jet to separate from the surface. Therefore, lift off occurs and the film cooling effectiveness decreases. In addition, the counter-rotating vortex pair becomes very strong for higher blowing ratio ($M = 2$) at different streamwise angles especially for $\alpha = 90$ degrees. This large mechanism structure reduces the exchange of the momentum and heat transfer between the jet and mainstream flow.

3.3.3. Effect of Lateral and Forward Diffusion Angles on Average Overall Film Cooling Effectiveness. Three holes of different lateral and diffusion angles are investigated. The non dimensional average wall temperature or average overall film

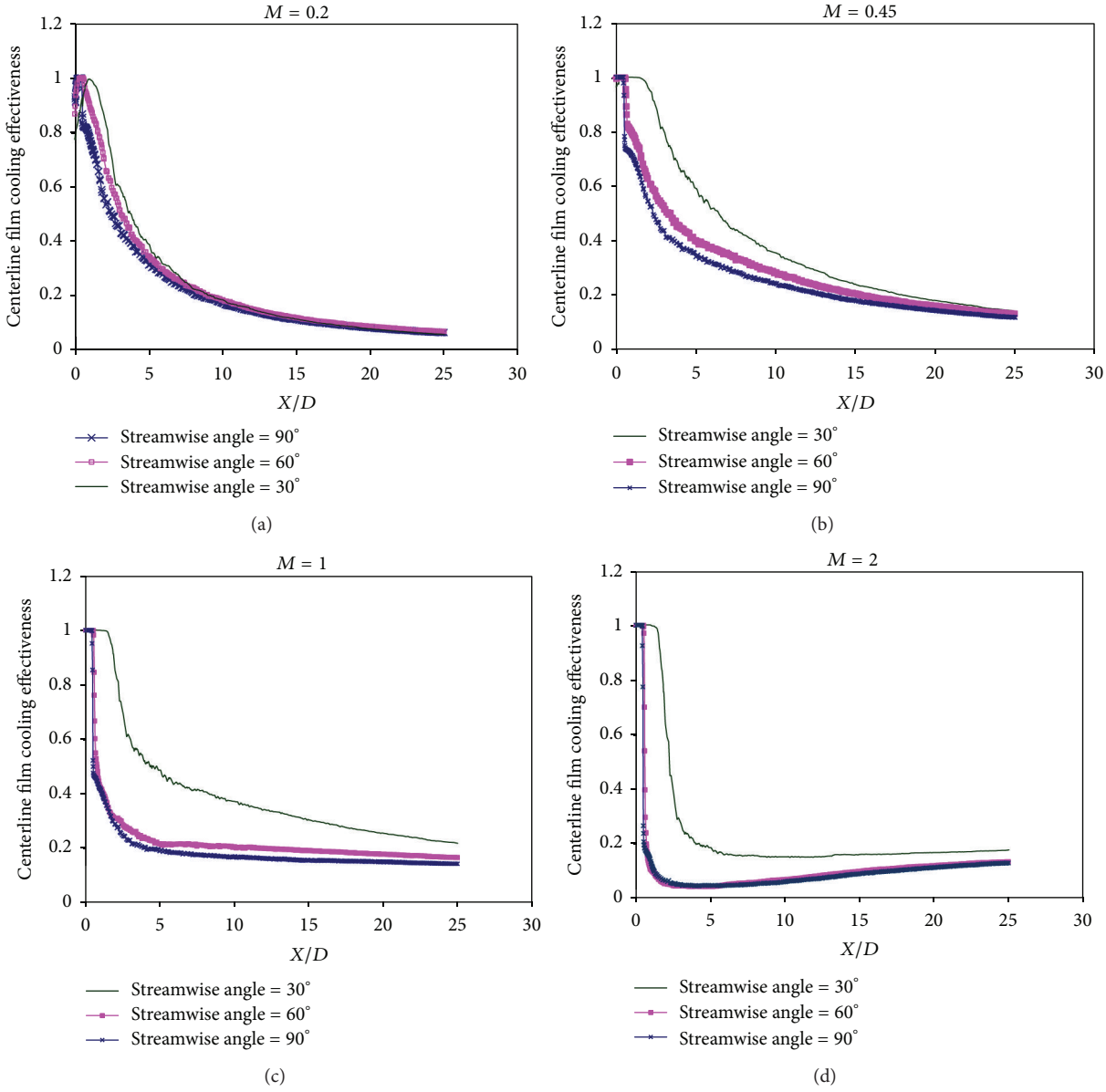

Figure 28: Variation of the centerline effectiveness with X/D for LFDSA-0-0.

cooling effectiveness is presented in Figure 30 for holes of equal lateral and diffusion angles of 0, 10, and 15 degrees. The results indicate that the average overall film cooling effectiveness increases rapidly with increasing the blowing ratio up to certain value. At this value better mixing and good cooling in streamwise and spanwise which minimize the average wall adiabatic temperature thus average overall film cooling effectiveness. By increasing the blowing ratio more than the value which gives a maximum average effectiveness, the lift off begins to appear on the flat plate. The optimum streamwise angle, which maximizes the average overall film cooling effectiveness, is 20 deg for three holes with different values of blowing ratio. The optimum blowing ratio which maximizes the average overall film cooling effectiveness at the optimum streamwise angle for these different holes is listed in Table 1. The target of this study minimizes the search area used in simplex optimization in order to minimize the iterations number.

4. Optimization Results

4.1. Simplex Optimization Results for Film Cooling on Flat Plate. The optimization procedure carried out requires the definition of a cost function. In this section, the results of flat plate optimization are presented. The objective or cost function is the average overall film cooling effectiveness defined in (2). Optimization results of the flat plate film cooling are presented in Table 2. The optimization results shown in Table 2 show that the optimum value of average

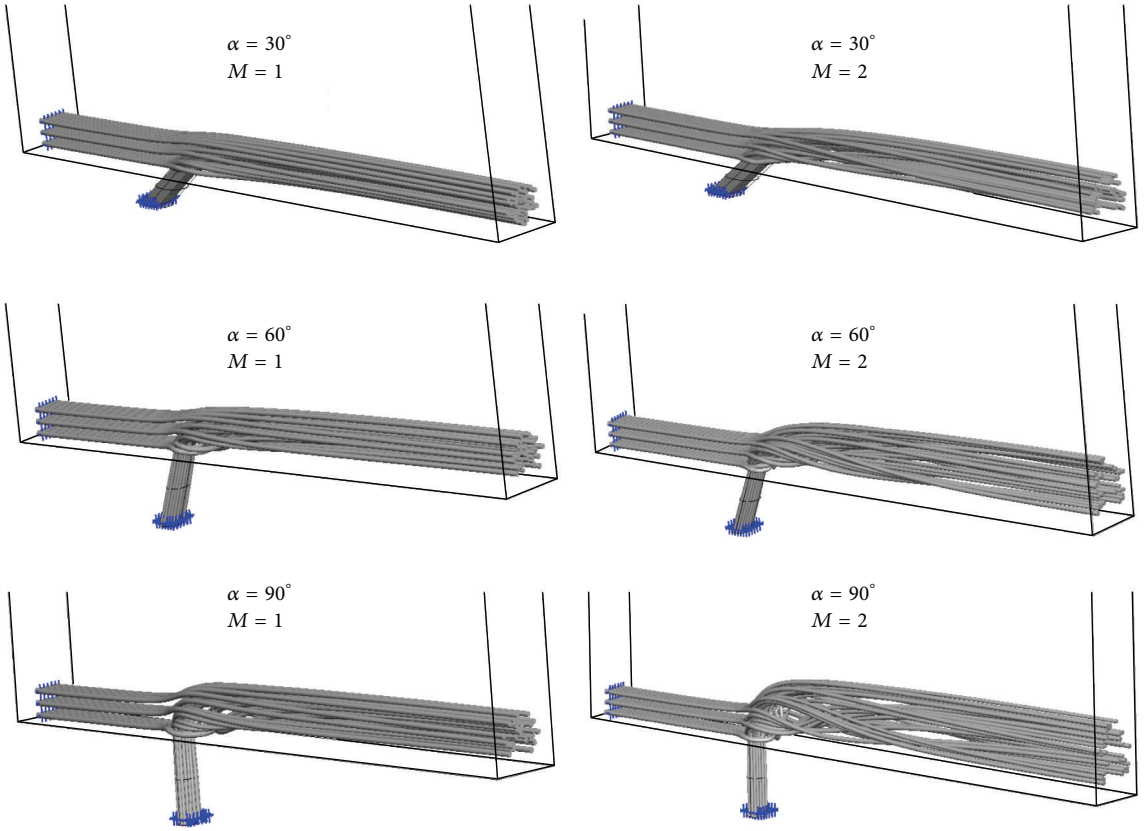

Figure 29: Stream tubes on flat plate with cylindrically hole shape (LFDSA-0-0).

Table 1: Average overall film cooling effectiveness at different blowing ratios.

Hole shape	Blowing ratio	Maximum average overall film cooling effectiveness
LFDSA-00-00	1.1	0.174
LFDSA-10-10	4.0	0.200
LFDSA-15-15	2.0	0.240

Table 2: Optimization results of flat plate film cooling.

Iteration number	A	δ	γ	M	$1/\eta_o$	η_o
27	20.99	14.55	9.33	1.78	4.102	0.2438

overall film cooling effectiveness is 0.244 for LFDSA-9.3-14.6 hole shape.

Figure 31 presents the variation of average overall film cooling effectiveness versus the number of iterations. An optimum value for the average overall film cooling effectiveness of 0.244 is obtained for LFDSA-9.3-14.6 hole shape, streamwise angle of 21 deg, and blowing ratio of 1.78. The top and symmetric planes effectiveness and temperature contours of the optimized hole shape are presented in Figure 32.

4.2. Film Cooling of Turbine Blade. The optimum LFDSA hole shape obtained from the flat plate simplex optimization is used for an actual turbine blade cooling. The turbine cooling is also done with a cylindrically and LFDSA-5-5 hole shapes, and the results are compared for the three hole shapes. The numerical calculations are performed for a *GE-E*^{3} turbine blade with a single suction side squealer tip to minimize the tip leakage flow.

Figure 33 shows the geometry for the *GE-E*^{3} blade with three arrays of cooling holes. The first array has eight LFDSA holes, and it is located on the blade pressure side at ten percent of the side length measured from the leading edge. The second array is located on the blade suction side at twenty-five percent of side length measured from the leading edge. The last array has a seven cylindrically hole shape and is located on the blade tip camber line. The computational domain consists of a single blade with periodic conditions imposed along the boundaries in the circumferential (theta) direction. A tip clearance of 1.5% of the blade span is assumed with squealer cavity of depth 2.1% of the blade span. The diameter of the inlet film cooling hole system is 0.127 cm and the flow injected with temperature is 923 K. The inlet boundary is placed at one-half chord length upstream of the blade so that the simple uniform inflow boundary conditions can be employed. A total temperature of 1700 K and total pressure of 1.675 MPa are specified with an inlet flow angle of 32 degrees. The inlet flow velocity is 183 m/sec. The exit boundary is located at one chord length downstream of the blade trailing edge to provide appropriate resolution of

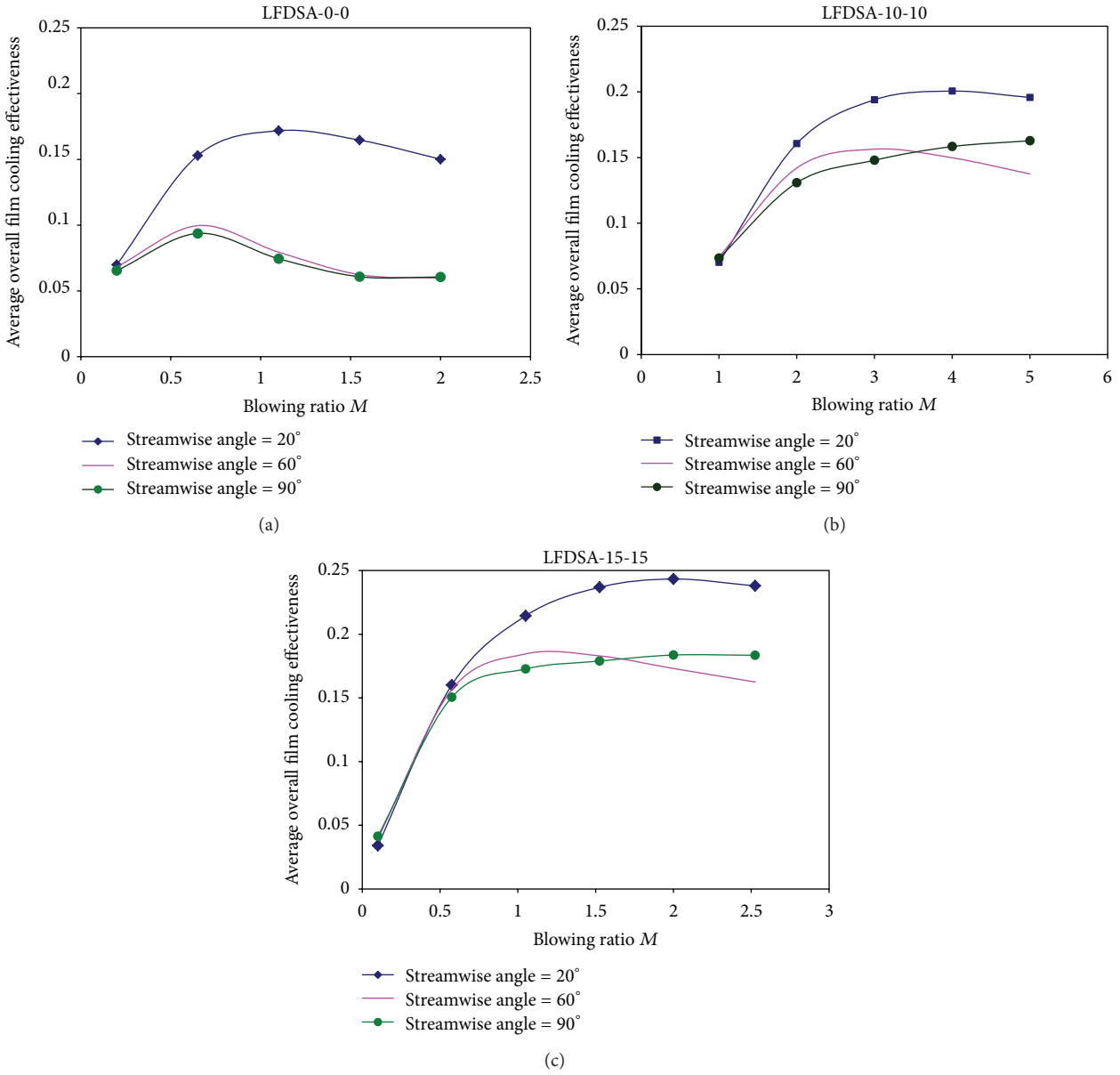

Figure 30: Average overall film cooling effectiveness versus blowing ratio for different streamwise angles of different hole shapes.

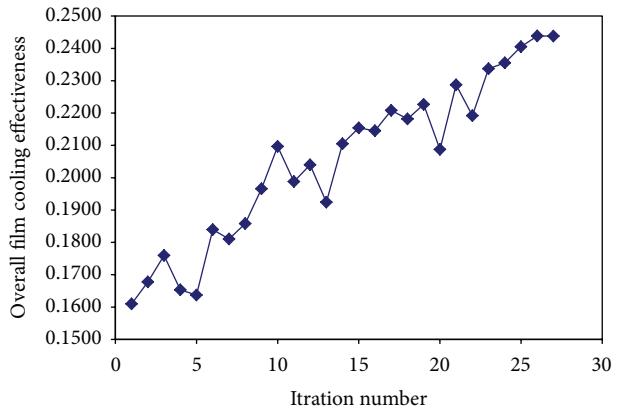

Figure 31: Optimization history of flat plate film cooling effectiveness.

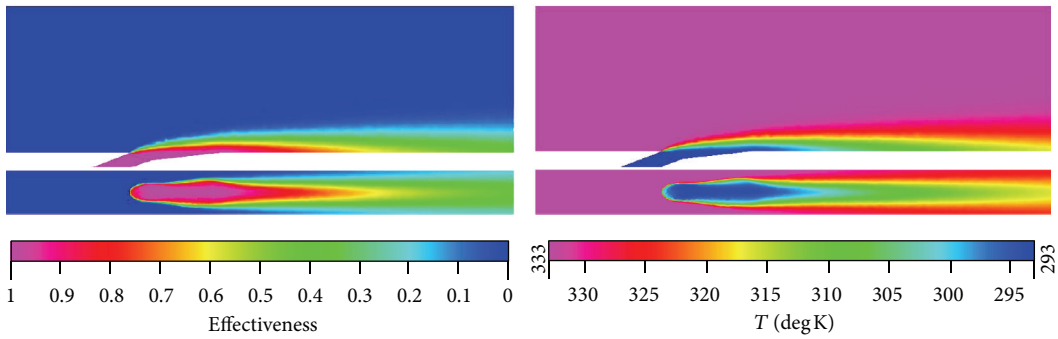

Figure 32: Effectiveness and temperature contours of flat plate film cooling for optimum hole shape.

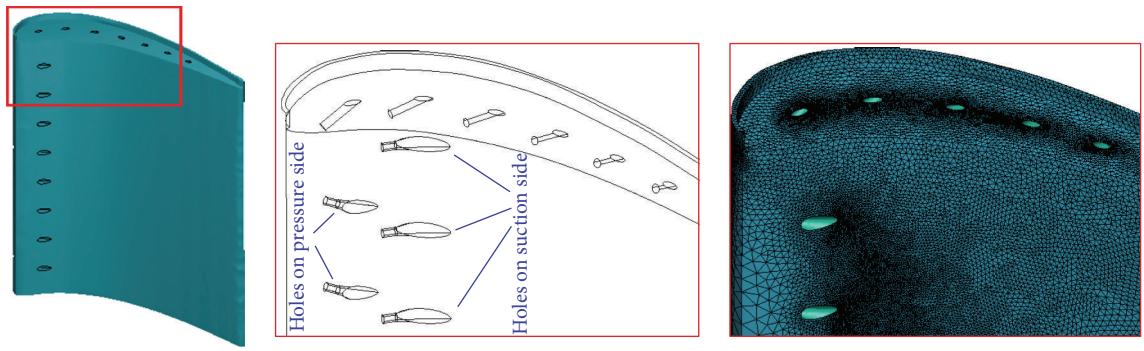

Figure 33: Actual turbine blade with LFDSA hole shape and blade unstructured grid.

the tip leakage flow and passage vortices. The static pressure is specified as 1.03 MPa at the exit. Therefore, the inlet total pressure to the outlet static pressure ratio (PR = $P_{in,t}/P_{out}$) is 1.63. On the blade surface, the no-slip condition is specified. A rotating speed of 9,600 rpm is used in the present simulation while the shroud remains stationary, as shown in Figure 34. The total number of cells used for the numerical simulations is 1.4 million cells with the same value of $y+$ obtained from the flat plate grid sensitivity on the blade surface.

The distribution of the blade cooling effectiveness for the three hole configurations is presented in Figure 35 for a blowing ratio of $M = 1.78$ and cylindrically hole shape on the blade tip. The coolant is injected with a streamwise angle of 21 degrees on the blade tip and the suction side. However, the injection angle of the coolant on the blade pressure side is taken to be 35 degrees because it is difficult to have an intersection between the cooling hole and the blade on the pressure side for a small streamwise angle and high forward angle (LFDSA case). Three different cases are simulated numerically for the computation of the film cooling effectiveness on the turbine blade. The first case is a turbine blade with cylindrically hole shape on the pressure and suction sides. The second case is a turbine blade with LFDSA-5-5 hole on the pressure and suction sides. The last case is a turbine blade with LFDSA-9.3-14.6 on the pressure and suction sides.

The results indicate that the effectiveness distribution on the pressure and suction sides changes significantly with the variation of the hole configuration. The highest effectiveness is obtained for a hole shape of configuration LFDSA-9.3-14.6. The blade overall film cooling effectiveness for these configurations is listed in Table 3.

Table 3: Comparison of turbine blade film cooling effectiveness for different hole shapes.

Hole shape	LFDSA-0-0	LFDSA-5-5	LFDSA-9.3-14.6
Turbine blade average overall film cooling effectiveness (η_o)	0.136	0.151	0.170

5. Conclusions

In the current work, optimization of film cooling parameters on a flat plate is investigated numerically. A parametric study is performed on the flat plate film cooling to determine the optimum parameters. The effect of film cooling parameters such as inlet velocity direction, lateral and forward diffusion angles, blowing ratio, and streamwise angle on the cooling effectiveness is studied, and optimum cooling parameters are selected. The numerical simulation of the coolant flow through flat plate hole system is carried out using the "CFDRC package" coupled with the optimization algorithm "simplex" to maximize the overall film cooling effectiveness. Unstructured finite volume technique is used to solve

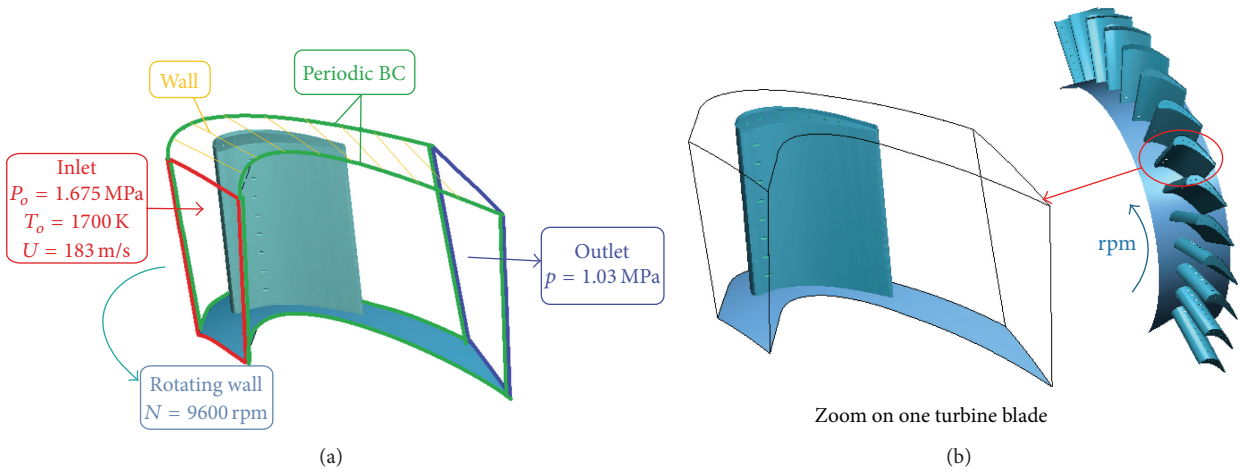

Figure 34: Turbine blade computational domain and boundary conditions.

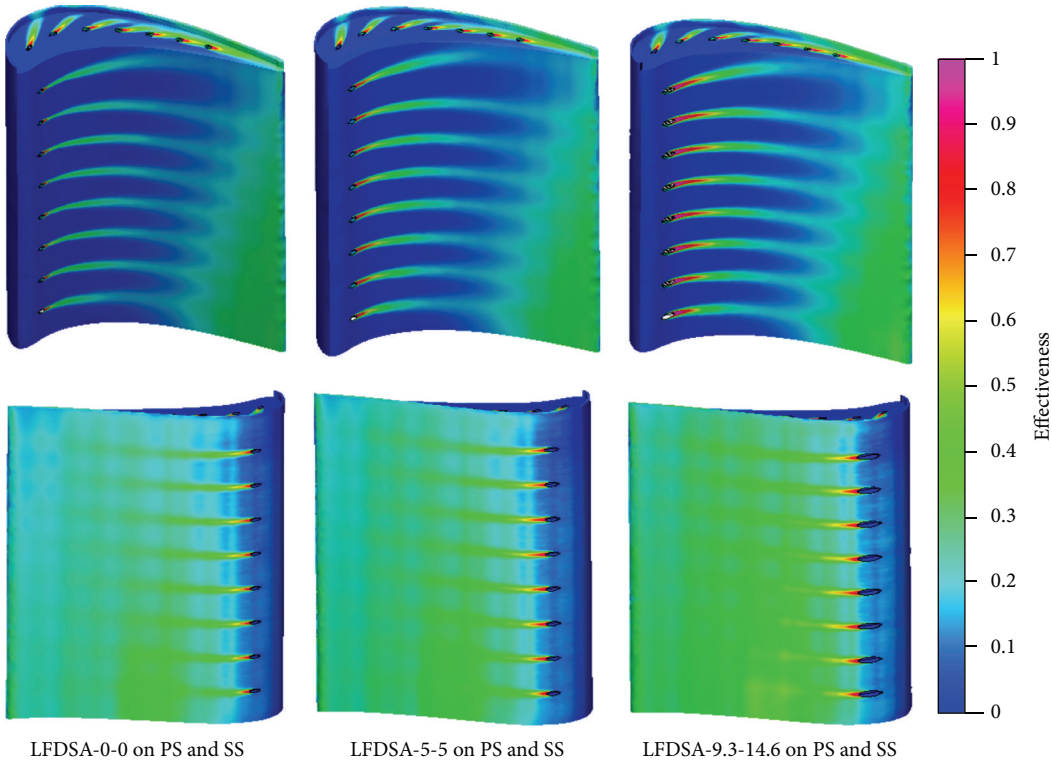

Figure 35: Effectiveness contours on the pressure and suction sides for different hole configurations.

the steady, three-dimensional and compressible Navier-Stokes equations. A grid sensitivity analysis is performed for the flat plate film cooling, and the results are compared with the published numerical and experimental data of a cylindrically round-simple hole. The results show good agreement with the published data. In addition, the results indicates that the overall film cooling effectiveness is enhanced by decreasing the streamwise angle for high blowing ratio and also by increasing the lateral and forward diffusion angles. The current study indicate that the hole should be designed such that the coolant flow is in the direction of the streamwise angle for high blowing ratio to reduce the lift off phenomena. An optimum geometry for cooling hole on a flat plate is determined. In addition, numerical simulations of film cooling on actual turbine blade are performed using the flat plate optimal hole geometry.

Nomenclature

D: Hole diameter, (m)
L: Hole length, (m)

L_1 : Hole metering section length, (m)
L_2 : Hole diffused section length, (m)
M: Blowing ratio, $(\rho_c v_c/\rho_h v_h)$
T : Wall temperature at any point, (K)
T_{av} : Average wall temperature, (K)
T_c : Temperature of coolant air, (K)
T_h : Temperature of hot air
$T_{\text{in},t}$: Turbine total inlet temperature, (K)
v_c : Velocity of coolant air, (m/s)
v_h : Velocity of hot gases, (m/s).

Greek Symbols

α: Streamwise (simple) angle
γ: Lateral injection angle
δ: Forward injection angle
η : Local film cooling effectiveness, $((T_h - T)/(T_h - T_c))$ or $((T_{\text{in},t} - T)/(T_{\text{in},t} - T_c))$
η_o : Average film cooling effectiveness, $((T_h - T_{\text{av}})/(T_h - T_c))$ or $((T_{\text{in},t} - T_{\text{av}})/(T_{\text{in},t} - T_c))$
ρ_c : Density of coolant air, (Kg/m^3)
ρ_h : Density of hot air, (Kg/m^3).

Abbreviations

LFDSA: Laterally and forwardly diffused simple angle
PS: Pressure side of turbine blade
SS: Suction side of turbine blade.

References

[1] D. P. Narzary, K. Liu, A. P. Rallabandi, and J. Han, "Influence of coolant density on turbine blade film-cooling using pressure sensitive paint technique," in *Proceedings of the ASME Turbo Expo*, Paper GT2010-22781, pp. 1529–1540, Glasgow, UK, June 2010.

[2] C. H. N. Yuen and R. F. Martinez-Botas, "Film cooling characteristics of a single round hole at various streamwise angles in a crossflow—part I: effectiveness," *International Journal of Heat and Mass Transfer*, vol. 46, no. 2, pp. 221–235, 2003.

[3] H. Nasir, S. Acharya, and S. Ekkad, "Improved film cooling from cylindrical angled holes with triangular tabs: effect of tab orientations," in *Proceeding of the IGTI*, New Orleans, La, USA, 2001.

[4] D. G. Bogard and K. A. Thole, "Gas turbine film cooling," *Journal of Propulsion and Power*, vol. 22, no. 2, pp. 249–270, 2006.

[5] R. S. Bunker, "Axial turbine blade tips: function, design, and durability," *Journal of Propulsion and Power*, vol. 22, no. 2, pp. 271–285, 2006.

[6] A. P. Rallabandi, J. Grizzle, and J. C. Han, "Effect of upstream step on flat plate film cooling effectiveness using PSP," in *Proceedings of the ASME Summer Heat Transfer Conference (HT '08)*, vol. 2, pp. 599–609, Jacksonville, Fla, USA, August 2008, HT08-56194.

[7] R. S. Bunker, "Film cooling effectiveness due to discrete holes within a transverse surface slot," ASME Paper GT-2002-30178, 2002.

[8] S. K. Waye and D. G. Bogard, "High-resolution film cooling effectiveness measurements of axial holes embedded in a transverse trench with various trench configurations," *Journal of Turbomachinery*, vol. 129, no. 2, pp. 294–302, 2007.

[9] P. M. Ligrani, J. M. Wigle, and S. W. Jackson, "Film-cooling from holes with compound angle orientations—part 2: results downstream of a single row of holes with 6d spanwise spacing," *Journal of Heat Transfer*, vol. 116, no. 2, pp. 353–362, 1994.

[10] K. Kusterer, D. Bohn, T. Sugimoto, and R. Tanaka, "Double-jet ejection of cooling air for improved film cooling," *Journal of Turbomachinery*, vol. 129, no. 4, pp. 809–815, 2007.

[11] R. J. Goldstein, E. R. G. Eckert, V. L. Eriksen, and J. W. Rarnsey, "Film cooling following injection through inclined circular tubes," *Israel Journal of Technology*, vol. 8, no. 1-2, pp. 145–154, 1970.

[12] S. Honami, T. Shizawa, and A. Uchiyama, "Behavior of the laterally injected jet in film cooling: measurements of surface temperature and velocity/temperature field within the jet," *Journal of Turbomachinery*, vol. 116, no. 1, pp. 106–112, 1994.

[13] S. W. Lee, Y. B. Kim, and J. S. Lee, "Flow characteristics and aerodynamic losses of film-cooling jets with compound angle orientations," *Journal of Turbomachinery*, vol. 119, no. 2, pp. 310–319, 1997.

[14] J. D. Denton, "Loss mechanisms in turbomachines," *Journal of Turbomachinery*, vol. 115, no. 4, pp. 621–656, 1993.

[15] P. M. Ligrani, J. M. Wigle, S. Ciriello, and S. M. Jackson, "Film-cooling from holes with compound angle orientations—part 1: results downstream of two staggered rows of holes with 3d spanwise spacing," *Journal of Heat Transfer*, vol. 116, no. 2, pp. 341–352, 1994.

[16] B. Sen, D. L. Schmidt, and D. G. Bogard, "Film cooling with compound angle holes: heat transfer," *Journal of Turbomachinery*, vol. 118, no. 4, pp. 800–806, 1996.

[17] D. L. Schmidt, B. Sen, and D. G. Bogard, "Film cooling with compound angle holes: adiabatic effectiveness," *Journal of Turbomachinery*, vol. 118, no. 4, pp. 807–813, 1996.

[18] S. V. Ekkad, D. Zapata, and J. C. Han, "Film effectiveness over a flat surface with air and CO_2 injection through compound angle holes using a transient liquid crystal image method," *Journal of Turbomachinery*, vol. 119, no. 3, pp. 587–593, 1997.

[19] S. V. Ekkad, D. Zapata, and J. C. Han, "Heat transfer coefficients over a flat surface with air and CO_2 injection through compound angle holes using a transient liquid crystal image method," *Journal of Turbomachinery*, vol. 119, no. 3, pp. 580–586, 1997.

[20] G. Medic and P. A. Durbin, "Toward improved film cooling prediction," *Journal of Turbomachinery*, vol. 124, no. 2, pp. 193–199, 2002.

[21] L. M. Wright, S. T. McClain, and M. D. Clemenson, "Effect of freestream turbulence intensity on film cooling jet structure and surface effectiveness using PIV and PSP," *Journal of Turbomachinery*, vol. 133, no. 4, Article ID 041023, 12 pages, 2011.

[22] S. Muppidi and K. Mahesh, "Direct numerical simulation of round turbulent jets in crossflow," *Journal of Fluid Mechanics*, vol. 574, pp. 59–84, 2007.

[23] S. Muppidi and K. Mahesh, "Direct numerical simulation of turbulent jets in crossflow," in *Proceedings of the AIAA 2005-1115 Aerospace Sciences Meeting and Exhibit*, pp. 4213–4228, January 2005.

[24] H. A. Daud, Q. L. Li, O. A. Beg, and S. S. A. Abdul Ghani, "Numerical investigation of film cooling effectiveness and heat

transfer along a flat plate," *International Journal of Applied Mathematics and Mechanics*, vol. 8, no. 17, pp. 17–33, 2012.

[25] D. Ai, P. Ding, and P. Chen, "Selection criterion of injection temperature pair for transient liquid crystal thermography on film cooling measurements," *International Journal of Heat and Mass Transfer*, vol. 44, no. 7, pp. 1389–1399, 2001.

[26] H. Nasir, S. Acharya, and S. Ekkad, "Film cooling from a single row of cylindrical angled holes with triangular tabs having different orientations," in *Proceeding of the IGTI*, New Orleans, La, USA, 2001.

[27] J. F. Kline, R. G. Stabe, and T. P. Moffitt, "Effect of cooling-hole geometry on aerodynamic performance of a film-cooling turbine vane tested with cold air in a tow-dimensional cascade," NASA-TP-1978-1136, Lewis Research Center, NASA, Cleveland, Ohio, USA, 1978.

[28] C. L. Liu, H. R. Zhu, and J. T. Bai, *Effect of Turbulent Prandtl Number on the Computation of Film-Cooling Effectiveness*, School of Engineering and Energy, Northwestern Polytechnical University Report, Xi'an, China, 2005.

[29] A. K. Sinha, D. G. Bogard, and M. E. Crawford, "Film-cooling effectiveness downstream of a single row of holes with variable density ratio," *Journal of Turbomachinery*, vol. 113, no. 3, pp. 442–449, 1991.